Clim. Past, 16, 245–263, 2020
https://doi.org/10.5194/cp-16-245-2020

Climate of the Past
Open Access
EGU

Algal lipids reveal unprecedented warming rates in alpine areas of SW Europe during the industrial period

Antonio García-Alix[1,2,3], Jaime L. Toney[2], Gonzalo Jiménez-Moreno[1], Carmen Pérez-Martínez[4], Laura Jiménez[4], Marta Rodrigo-Gámiz[1], R. Scott Anderson[5], Jon Camuera[6], Francisco J. Jiménez-Espejo[3], Dhais Peña-Angulo[7], and María J. Ramos-Román[6]

[1]Department of Stratigraphy and Paleontology, University of Granada, Granada, 18072, Spain
[2]School of Geographical and Earth Sciences, University of Glasgow, Glasgow, G12 8QQ, UK
[3]Instituto Andaluz de Ciencias de la Tierra (IACT), CISC-UGR, Armilla, 18100, Spain
[4]Department of Ecology and Institute of Water Research, University of Granada, Granada, 18072, Spain
[5]School of Earth and Sustainability, Northern Arizona University, Flagstaff, AZ 86011, USA
[6]Department of Geosciences and Geography, University of Helsinki, Helsinki, 00014, Finland
[7]Department of Geography, University of Zaragoza, Zaragoza, 50009, Spain

Correspondence: Antonio García-Alix (agalix@ugr.es)

Received: 5 August 2019 – Discussion started: 21 August 2019
Revised: 20 December 2019 – Accepted: 9 January 2020 – Published: 6 February 2020

Abstract. Alpine ecosystems of the southern Iberian Peninsula are among the most vulnerable and the first to respond to modern climate change in southwestern Europe. While major environmental shifts have occurred over the last ∼ 1500 years in these alpine ecosystems, only changes in the recent centuries have led to abrupt environmental responses, but factors imposing the strongest stress have been unclear until now. To understand these environmental responses, this study, for the first time, has calibrated an algal lipid-derived temperature proxy (based on long-chain alkyl diols) to instrumental historical data extending alpine temperature reconstructions to 1500 years before present. These novel results highlight the enhanced effect of greenhouse gases on alpine temperatures during the last ∼ 200 years and the long-term modulating role of solar forcing. This study also shows that the warming rate during the 20th century (∼ 0.18 °C per decade) was double that of the last stages of the Little Ice Age (∼ 0.09 °C per decade), even exceeding temperature trends of the high-altitude Alps during the 20th century. As a consequence, temperature exceeded the preindustrial record in the 1950s, and it has been one of the major forcing processes of the recent enhanced change in these alpine ecosystems from southern Iberia since then. Nevertheless, other factors reducing the snow and ice albedo (e.g., atmospheric deposition) may have influenced local glacier loss, since almost steady climate conditions predominated from the middle 19th century to the first decades of the 20th century.

1 Introduction

Global mean annual surface temperatures have risen by ∼ 0.85 °C from 1880 to 2012, and the recent decades have been the warmest in the Northern Hemisphere during the Common Era (IPCC, 2013). This trend is alarming, since over the last decade record temperatures have been broken yearly. For example, in Spain the highest temperatures ever recorded in September and July occurred in 2016 (45.5 °C) and 2017 (46.9–47.3 °C), respectively (Spanish National Weather Agency – AEMet Open Data, 2019). Increasing global temperatures is contributing not only directly to land and ocean surface warming but also indirectly by changing the global hydrological cycle through the disturbance of atmospheric circulation patterns and moisture (Easterling et al., 2000; IPCC, 2013). As a result, the term "global warming" is migrating towards recent "climate change" in order to express the variety of modern climate extremes witnessed across the world. The effects of modern global warming and associated climate change events may be causing extreme environmental impacts, beyond what is recorded in the recent

geologic record (Waters et al., 2016). Hence, it is crucial to identify warming thresholds, rates, and forcing mechanisms from past high-resolution temperature records to understand modern climate change. It is especially important in fragile regions such as high-elevation ecosystems of the Mediterranean alpine realm, an environmentally vulnerable biodiversity "hot spot" (Giorgi, 2006; Schröter et al., 2005) where recent climate change is affecting species richness and distribution (Médail and Quézel, 1999; Pauli et al., 2012). Therefore, alpine wetlands in the Mediterranean region, such as the ones from the Sierra Nevada in the southern Iberian Peninsula, are sensitive recorders of changing climate, and their sedimentological records archive the ecological and biogeochemical responses to different environmental forcings (Catalan et al., 2013).

In order to contribute to a better understanding of recent climate change events in these vulnerable areas, here, for the first time, we calibrate a recently developed algal lipid-derived temperature proxy in an alpine lacustrine record that overlaps with instrumental temperature time series. This calibration allows for the reconstruction of temperatures in alpine areas of the southern Iberian Peninsula during the Common Era when instrumental records are discontinuous or nonexistent. Temperature-dependent biomarkers, such as those produced by algae (alkenones) or bacteria/archaea (glycerol dialkyl glycerol tetraethers: GDGTs) have been commonly used in a wide range of marine records as quantitative paleothermometers, and their further application in lake environments has widely increased in the last decade (e.g., Castañeda and Schouten, 2011; Colcord et al., 2015; Foster et al., 2016; Longo et al., 2018; Theroux et al., 2010). Another promising type of algal lipid biomarkers, the long-chain alkyl diols (hereafter LCDs), has also been assessed as a temperature proxy in marine environments (Rampen et al., 2012, 2014b; Rodrigo-Gámiz et al., 2014, 2015). Nevertheless, the relationship between LCDs and temperature has only been tentatively tested in freshwater environments (Rampen et al., 2014a). In this regard, studies using LCDs as (paleo)environmental proxies in marine environments (not just for temperature reconstructions) have increased in the last years, showing the potential of LCDs as proxies for upwelling (Rampen et al., 2008; Versteegh et al., 1997; Willmott et al., 2010), riverine inputs to marine settings (de Bar et al., 2016; Lattaud et al., 2017a, 2018a), or nutrient inputs (Gal et al., 2018). Nevertheless, only a few studies have tested LCDs as lacustrine archives of paleoproductivity (Shimokawara et al., 2010), past rainfall anomalies (Romero-Viana et al., 2012), or temperatures (Rampen et al., 2014a), among others. In any case, despite the great potential of LCDs for paleoenvironmental reconstructions, a number of questions exist about the applicability of diols in high-latitude areas (Rodrigo-Gámiz et al., 2015), in freshwaters records (Rampen et al., 2014a), and about the distribution and sources of the biological producers (Balzano et al., 2018; Villanueva et al., 2014; Yu et al., 2018).

The LCD distribution in marine environments shows significant correlations with mean annual sea surface temperature through the ratio of the fractional abundances of C_{28} 1,13-diol, C_{30} 1,13-diol, and C_{30} 1,15-diol that are used in the long-chain diol index (LDI, Eq. 1) (Rampen et al., 2012). The application of LCDs as a temperature proxy is novel in freshwater environments and only two preliminary calibrations based on recent surface sediments have been obtained using both mean annual air temperatures (weather station data) and organic-derived temperature proxies (GDGTs) (Rampen et al., 2014a). Here, we improve the biomarker paleothermometry by establishing the first temperature calibration for freshwater LCDs using a comparison with historical temperature records for the last $\sim$ 100 years. Although this calibration can only be applied to the studied lake at present, and perhaps to other alpine wetlands in the Sierra Nevada area, these new data support and reinforce the promising use of LCDs as a paleotemperature proxy in freshwater environments.

$$\mathrm{LDI} = (\mathrm{F_{C30}}1,15\text{-diol})/(\mathrm{F_{C28}}1,13\text{-diol} + \mathrm{F_{C30}}1,13\text{-diol} + \mathrm{F_{C30}}1,15\text{-diol}) \text{ (Rampen et al., 2012)} \quad (1)$$

Regional settings

This paper focuses on the LCD record of two adjacent cores from Laguna de Río Seco (LdRS), a small alpine lake ($\sim$ 0.42 ha and less than 3 m of water depth) at 3020 m a.s.l. in the protected Sierra Nevada National Park, southern Spain (Fig. 1). Alpine Sierra Nevada wetlands, including LdRS, are low-primary-production (oligo to mesotrophic) systems, and their biogeochemical cycles partially depend on eolian nutrient supplies (e.g., Saharan aerosol deposition), since catchment basins are small and barren in nutrients (Morales-Baquero et al., 2006; Pulido-Villena et al., 2005; Reche et al., 2009).

Sierra Nevada is the southwestern-most mountain range in Europe, where latest Pleistocene cirque glaciers carved the metamorphic (mica schist) bedrock in the highest peaks (Castillo Martín, 2009). Massive glacier melting at the latest Pleistocene–Holocene transition transformed the former glacial depressions into lacustrine areas (Castillo Martín, 2009) that evolved gradually into either shallow lakes or peatlands around the middle-to-late Holocene transition (Garcia-Alix et al., 2017; Jiménez-Espejo et al., 2014). Small glaciers reappeared at the highest peaks of the Sierra Nevada in the 15th century, during the Little Ice Age (LIA), and remained until the 20th century (Oliva et al., 2018). The presence of these glaciers is observed in the sedimentary record of some alpine lakes and wetlands in the Sierra Nevada as deposit of coarse sediments, like Laguna de la Mosca on the north face of the Sierra Nevada (Oliva and Gomez-Ortiz, 2012). However, these kinds of deposits have not been registered in LdRS (south face of the Sierra Nevada), where the

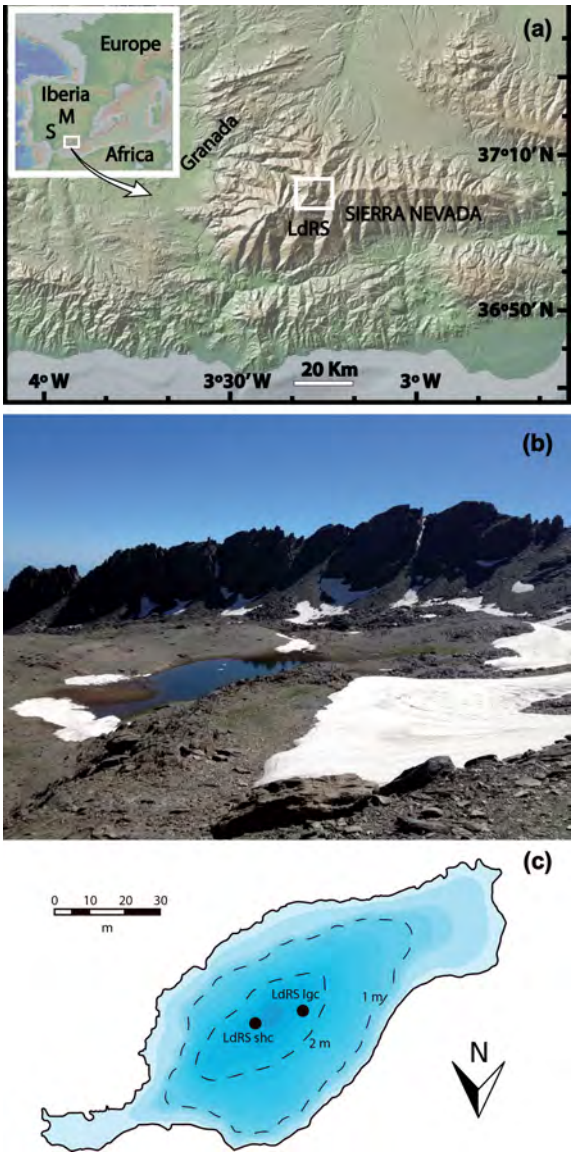

Figure 1. Geographical setting. **(a)** Location of the Sierra Nevada in the western Mediterranean region: Madrid (M), Seville (S), and Granada observatories, as well as the studied area Laguna de Río Seco (LdRS); **(b)** LdRS catchment basin (0.42 ha) in spring 2013; **(c)** bathymetry map of LdRS along with the sampling points of both cores. Data source and software: **(a)** map created by Antonio García-Alix using GeoMapApp (3.6.6) (http://www.geomapapp.org, last access: 19 December 2019); **(b)** picture from Antonio García-Alix; **(c)** digitalized map of a bathymetry report from Egmasa S.A.

last 1500 years are characterized by continuous laminated clays and bryophyte layers (Anderson et al., 2011). Glacial effects have not caused any disturbance on wetland sedimentation (e.g., erosion), and local alpine sedimentary records show continuous sedimentation patterns (Anderson et al., 2011; García-Alix et al., 2012; Jiménez-Moreno and Anderson, 2012; Jiménez-Moreno et al., 2013; Mesa-Fernández et al., 2018; Oliva and Gomez-Ortiz, 2012; Ramos-Román et al., 2016). Conversely, an increase in sedimentation rates have been detected in the last ∼ 200 years, probably resulting from the waning stages of the LIA (Oliva and Gomez-Ortiz, 2012) and enhanced human activities in the alpine areas of Sierra Nevada during the 19th (García Montoro et al., 2016; Titos Martínez, 2019; Titos Martínez and Ramos Lafuente, 2016) and 20th (Jiménez et al., 2015) centuries. These high-sedimentation rates did not affect the natural responses of the local algal communities to environmental variables such as temperature, but there has been a dilution effect of algal compounds (e.g., chlorophyll and labile carotenoids) in the sediments (Jiménez et al., 2015).

During the 20th century this sensitive alpine region of southern Iberia has experienced significant impacts from modern climate change as evidenced, for example, by the first permanent European glacier loss there during the first half of the 20th century (Grunewald and Scheithauer, 2010) and the extreme permafrost reduction during recent decades (Oliva and Gomez-Ortiz, 2012). This melting supplied a large volume of freshwater (Jiménez et al., 2019) that boosted the water availability in the area and the occasional development of local aquatic environments, contrasting with the general environmental aridification trend observed throughout the 20th century (Garcia-Alix et al., 2017; Jiménez et al., 2019; Ramos-Román et al., 2016).

The sedimentary archive of LdRS has been selected for this study in order to (1) improve the freshwater LCD paleothermometry by proposing a new temperature calibration for freshwater LCDs in the alpine wetlands of the Sierra Nevada area, (2) reconstruct temperatures beyond the instrumental record in a site at the leading edge of changing climate, (3) assess the role of different radiative forcing (e.g., solar radiation or greenhouse gas concentrations) on temperature change in alpine wetlands of southwestern Europe during the Common Era, and (4) understand the responses to recent climate change in this highly sensitive environment.

2 Materials and methods

2.1 Sediment sampling

Two sediment cores were taken at the deepest part of LdRS, an alpine lake at 3020 m a.s.l. in the Sierra Nevada (southern Iberian Peninsula) (Fig. 1). A long sediment core (150 cm) was retrieved in 2006 (LdRS lgc). A short sediment core of 16 cm was collected in 2008 (LdRS shc) using a slide-hammer gravity corer (Aquatic Research Instruments, Hope, Idaho, USA). Independent age models were performed in each sediment core to avoid potential correlation problems caused by changes in the sedimentation rates between both coring sites (Fig. 1c) and different sampling dates (2006 LdRS lgc and 2008 LdRS shc). The age model of LdRS lgc is based on ^{210}Pb and ^{137}Cs in the uppermost part (first 15 cm) and ^{14}C analyses in older sediments (Anderson et

al., 2011). The age model of the LdRS shc is based on gamma spectroscopy by measuring the ^{210}Pb, ^{137}Cs, and ^{226}Ra radionuclides in the first ∼ 14 cm; afterwards, the age was extrapolated to the core bottom (16 cm) (Jiménez et al., 2018, 2019). Both records show that the sediment accumulation rate for the uppermost 15–16 cm ranges between 0.09 and 0.13 cm yr^{-1} (Anderson et al., 2011; Jiménez et al., 2018), with lower sedimentation rates below this depth (∼ 0.008 cm yr^{-1}) (Anderson et al., 2011). Age models show that the LdRS shc extends back to ∼ 200 years with a sample resolution ranging from 5 to 7 years (high resolution) (Jiménez et al., 2018, 2019). In the case of the LdRS lgc, the section studied in this paper covers the last ∼ 1500 years with a lower sample resolution. In this case, the sample resolution is around 6–7 years in the first 10 cm and from 24 to 150 years in older samples (Anderson et al., 2011).

2.2 Geochemical analyses

Thirty-two sediment samples were collected consecutively every 0.5 cm along LdRS shc and 21 samples in the first 22 cm of LdRS lgc. The samples were freeze-dried and homogenized. The total lipid content was extracted from the sediment samples using a Thermo Scientific™ Dionex™ ASE™ 350 accelerated solvent extractor system at 100 °C and 7×10^6 Pa using a mixture of dichloromethane (DCM) and methanol (9 : 1, $v : v$). Afterwards, the neutral fraction was separated by means of aminopropyl silica gel chromatography using DCM–isopropanol (1 : 1, $v : v$). This neutral fraction was subsequently eluted with hexane, DCM, ethyl acetate–hexane (25 : 75, $v : v$), and methanol through a 230–400 mesh (35–70 µm) silica gel chromatographic column in order to obtain four neutral subfractions (N1–N4). Long-chain diols were obtained in the third neutral fraction (N3, alcohol fraction), which was derivatized by bis-(trimethylsilyl) trifluoroacetamide (BSTFA) before running the analyses. Volumes of 30 µL of BSTFA and 40 µL of pyridine were added to each N3 fraction and heated at 80 °C for 2 h. When vials were at room temperature, a volume between 140 and 220 µL of DCM was added to each sample. Firstly, the derivatized N3 fractions were analyzed with gas chromatography with a flame ionization detector (GC-FID, Shimadzu 2010). An external standard of cholesterol was measured every five samples in order to estimate the appropriate concentration for mass spectrometry analyses. The sample at 19.5 cm depth in the long core was discarded because its concentration was below detection limits. Subsequently, the N3 fractions were measured in a Shimadzu QP2010 Plus mass spectrometer interfaced with a Shimadzu 2010 GC using a scan mode between m/z 50–650 in order to obtain a general picture of the mass spectrum of the samples and the specific retention times where the C_{28}, C_{30}, and C_{32} diols eluted. Afterwards, samples were reanalyzed on the basis of a selected ion monitoring mode (SIM), selecting the characteristic fragment ions of the most important long-chain diols, i.e., m/z 299, 313, 327, and 341 (Rampen et al., 2012; Versteegh et al., 1997) and the specific retention time window to identify the C_{28}, C_{30}, and C_{32} diols with the mid-chain alcohol positioned at carbon 13, 14 or 15. Fractional abundances of the C_{28} 1,13-diol, C_{30} 1,13-diol, C_{30} 1,15-diol were used in Eq. (1) to calculate the long-chain diol index (LDI) (Rampen et al., 2012). Fractional abundances of C_{28} 1,13-diol, C_{30} 1,13-diol, C_{30} 1,15-diol, and C_{32} 1,15-diol were used to characterize the potential diol source (e.g., marine, lacustrine, or specific algae groups) (Lattaud et al., 2018a; Rampen et al., 2014a). Fractional abundances of the C_{28} and C_{30} 1,14-diols were measured only in the short core in order to assess their potential relationship with temperatures (Rampen et al., 2014b). The presence of the $C_{32:1}$ 1,15-diol has also been tested, but it was only identified in some samples from the short core at very low concentrations, thus it is not included it in this study.

2.3 Reference temperature time series for LCD temperature calibrations

Generating an accurate temperature calibration based on LCDs in alpine wetlands from the Sierra Nevada area is challenging because there is a lack of long and continuous temperature time series at such high elevations. The meteorological observatories at the Sierra Nevada ski resort (ranging in elevation from 2500 to 3020 m a.s.l.) only provided discontinuous temperature records from 1965 to 2011 (Observatorio del cambio global de Sierra Nevada, 2016; Spanish National Weather Agency – AEMet Open Data, 2019) that show a significant correlation ($r > 0.95$; $p < 0.0001$) with low-elevation temperature time series (Tables S1, S2 in the Supplement). Therefore, a potential way to obtain a LCD-based temperature calibration is by means of the correlation of LCD data with long and reliable historical temperature time series at nearby lower-elevation areas, followed by a correction for the altitudinal effect on temperatures.

The three weather observatories in the Granada area, at the foothills of the Sierra Nevada, only provide reliable temperature data from the 1970s onwards (Spanish National Weather Agency – AEMet Open Data, 2019), which is a short period for an accurate downcore proxy calibration. Temperature time series preceding the 1970s have been reconstructed using statistical models (e.g., Gonzalez-Hidalgo et al., 2015), and they show a good correlation with the LDI and the relative abundances of the C_{28} 1,13-, C_{30} 1,13-, and C_{32} 1,15-diols, but a weaker correlation with the C_{30} 1,15-diol (Table S3). However, these correlations are weaker than the ones obtained from the Sevilla-Tablada observatory (hereafter Seville observatory) and Madrid-Retiro observatory (hereafter Madrid observatory). These observatories registered longer and more reliable temperature data than those obtained in Granada, which are likely biased by the quality of the reconstructed temperature data. Therefore, after testing the correlations between LCDs and different low-elevation

observatories (Table S3), we decided to develop the LCD-based temperature calibrations against the temperature time series from Seville and Madrid observatories. These observatories show the best correlations with the LCD data in addition to being the most reliable and longest temperature time series in the region (see Table S3 for further explanations and Fig. 1a for the location of these low-elevation observatories).

Another question to clarify in the study records before selecting the reference temperature time series for the LCD calibration is the potential seasonal effect on the LCD distributions, since different studies have shown diverse relationships between annual or seasonal temperatures and the LCDs. For example, good correlations have been found in marine environments between the fractional abundances of LCDs (expressed as LDI in all the cases) and annual (Rampen et al., 2012), winter and annual (Smith et al., 2013), or autumn and annual sea surface temperatures (Lattaud et al., 2018b). Despite fewer studies on the LCD distribution in freshwater environments, Rampen et al. (2014a) found a good correlation between the LCD distributions in a suite of lake surface sediments and mean summer lake temperatures (deduced from GDGTs). Nevertheless, the direct correlation between these LCD distributions and annual or seasonal air temperatures was weaker, probably due to the location of the weather observatories with respect to each study area. Villanueva et al. (2014) also investigated this seasonal effect and detected changes in the LCD distribution throughout the year in the water column and surface sediments from an African lake that could be either related to successive and different LCD-producer blooms or seasonal variations in the LCD production by a unique source. Both scenarios might affect LCD-based temperature reconstructions.

Considering all these constrains to select the best temperature time series to establish an accurate LCD-based temperature calibration, the most rigorous approach for the studied alpine site would consider annual and monthly water and/or air temperatures of the catchment basin at 3020 m a.s.l., as well as the periods of the year when the LCDs are produced, but these data are not available so far. Thus, the effect of seasonality has been estimated by means of the comparison with reliable seasonal long temperature time series from lower-elevation sites. In this regard, seasonal air temperatures for the last $\sim$ 100 years registered in Madrid and Seville observatories correlate with the LCD distributions (with a weaker correlation for the C_{30} 1,15-diols) and the LDI ($0.9 > r > 0.6$; $p < 0.001$). Nevertheless, this correlation is generally lower than the one obtained when considering only mean annual air temperatures (MAATs) (i.e., in the case of the LDI vs. MAAT $r = 0.9$; $p < 0.0001$). Since warm temperatures influence the algae growth in the studied area (Carrillo et al., 1991; Sánchez-Castillo, 1988), we would expect a higher correlation between LCDs and mean seasonal air temperatures from the warmer months (MWAT: May–September), which is potentially the LCD production season, but this correlation is lower than the annual ones in the case of the LDI (LDI vs. MWAT $0.8 > r > 0.7$; $p < 0.0001$) (Tables S3, S4). A similar pattern is observed when annual and warm season temperatures are compared with the fractional abundances of the C_{28} 1,13-, C_{30} 1,13-, C_{30} 1,15-, and C_{32} 1,15-diols (Table S3). Consequently, in view of (1) the fact that this is the first attempt at a freshwater LCD-based temperature calibration in this area; (2) there exists a high correlation between the different instrumental time series of regional air temperatures (seasonal vs. annual), and (3) the best correlations (normal and detrended) between the LCD distributions and temperatures are obtained when using MAAT (Tables S3, S4), we use MAAT for the LCD-based temperature calibrations in this study. Nevertheless, further work, including a monitoring program for monthly air temperatures in the catchment area and water temperatures in the lake, as well as suspended particulate matter and sediment trap studies, is required to better understand the local LCD production, improve the LCD-based temperature calibration, and minimize the uncertainties of the current approach.

Two groups of reference temperature time series at 3020 m a.s.l., based on the same batch of data, have been estimated in order to overcome the scarcity of high-elevation temperature time series in the Sierra Nevada and obtain a reliable mean LCD-based temperature calibration: (1) based on the elevational gradient between low- and high-elevation observatories and (2) based on the direct correlation between temperature time series from Madrid and Seville observatories and that at 3020 m a.s.l. (Cetursa 5 observatory) in the Sierra Nevada, which is near LdRS and at the same elevation (Table S1).

Reference temperature time series 1. The environmental lapse rate ($\Delta_{\text{temperature}}/\Delta_{\text{elevation}}$ in $^{\circ}\text{C m}^{-1}$) between lower-elevation observatories (with long temperature time series: Granada, Seville, and Madrid) and those from Sierra Nevada at higher elevation (with shorter temperature time series: Albergue and Cetursa 1, 3, and 5) has been estimated in order to correct the elevational gradient between them (more than 2200 m: Table S1). Due to few annual data points from high-elevation sites, monthly and annual (12 continuous months) environmental lapse rates were calculated to compare both datasets. The calculated temperature shifts between the reference low-elevation observatories and LdRS site at 3020 m a.s.l., worked out from the Supplement equations in Fig. S1 (Table S5), were applied to the temperature time series from Madrid and Seville for the last $\sim$ 100 years in order to obtain two reference temperature reconstructions (from 1908 to 2008 CE) at 3020 m a.s.l.: reference temperature time series 1a (from Madrid data) and reference temperature time series 1b (from Seville data).

Reference temperature time series 2. The direct comparison between Madrid and Seville temperatures and those from the observatory Cetursa 5 (3020 m a.s.l.) by means of ordinary least square regressions has given rise to two equations (Fig. S2a and b) that allow the reconstruction of temperature time series at 3020 m a.s.l. from 1908 to 2008: reference

temperature time series 2a (from Madrid data) and reference temperature time series 2b (from Seville data).

As a result, we have obtained four reference temperature time series at 3020 m a.s.l. where the effect of the altitudinal difference between low-elevation observatories (Madrid and Seville) and LdRS have been corrected by two different methods. Consequently, these four reference temperature series are highly similar, showing a certainly high correlation ($r > 0.98$; $p < 0.0001$), without significant difference between the sample medians (deduced from a Kruskal–Wallis test), and very low standard deviation between samples from the same time interval (SD < 0.2).

3 Results

3.1 Long-chain diols in the LdRS records

Six main LCD isomers have been identified and relative abundances analyzed in the LdRS cores: C_{28} and C_{30} 1,13-diols, C_{28} and C_{30} 1,14-diols, and C_{30} and C_{32} 1,15-diols. The LCD abundance changes through time in both records, but the C_{32} 1,15-diol is the predominant isomer in most of the samples. Nevertheless, the relative abundance of the C_{32} 1,15-diol drops abruptly (relative abundances between 25 % and 40 %) during the LIA, contrasting with a relative increase in the C_{28} and C_{30} 1,13-diols (Fig. 2). This switch in the most abundant isomers can be read as either a change in the LCD producers or an adaptation to colder temperatures of the same organism, and thus affecting the LCD production. Conversely, the C_{28} and C_{30} 1,14-diols show the lowest relative abundances (1.3 ± 0.4 % and 1.8 ± 0.3 %, respectively), and they were only quantified in the short core to assess their potential application as paleothermometer in LdRS. Although they show a good correlation with temperatures (C_{28} 1,14-diol: $0.66 > r > 0.45$ $p < 0.04$; C_{30} 1,14-diol: $-0.82 < r < -0.53$ $p < 0.02$), their low relative abundance, very close to the detection limit, together with a different biological source (Sinninghe Damsté et al., 2003), precludes us from including them in the temperature calibration and, therefore, in the discussion of this study. Consequently, the interpretations in this paper are only focused on the distribution pattern of the relative abundances of the main LCDs in LdRS: C_{28} and C_{30} 1,13-diols and C_{30} and C_{32} 1,15-diols.

The relative abundances of these four isomers in LdRS correlate well in both short and long cores; only the C_{30} 1,15-diol shows weaker correlations with the other isomers (Table S6). Overall, the C_{28} and C_{30} 1,13-diols show opposite trends to those from the C_{30} and C_{32} 1,15-diols. Their general trends for the last ~ 100 years seem to be influenced by the temperature oscillations at 3020 m a.s.l. (Table S7): the C_{28} and C_{30} 1,13-diols display a negative correlation with temperatures ($r < -0.7$ $p < 0.0001$) and the C_{32} 1,15-diol a positive one ($r > 0.8$ $p < 0.0001$). Although the C_{30} 1,15-diol also shows a positive relationship with temperatures, this correlation is weak ($r > 0.3$ $p < 0.0001$). Accordingly, the LDI values from LdRS for the last ~ 100 years show a significant correlation ($r > 0.9$ $p < 0.0001$) with the reference temperature time series at 3020 m a.s.l. (Table S7).

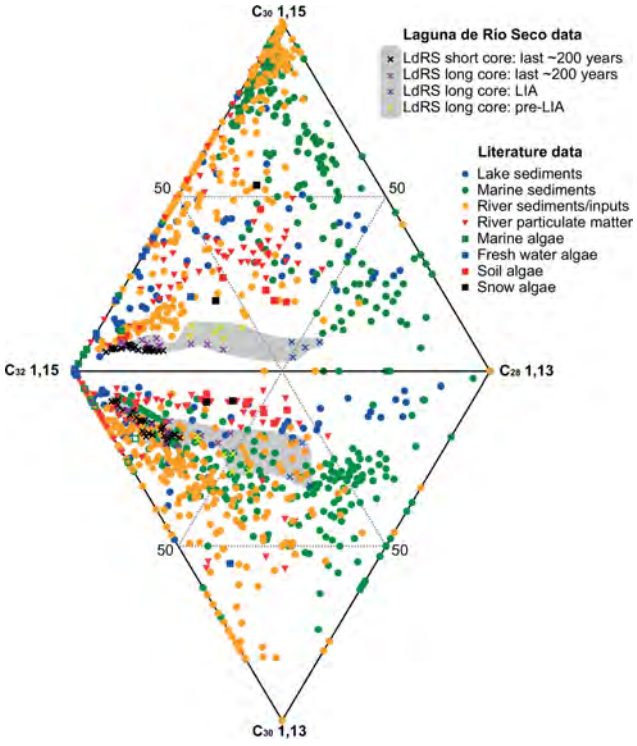

Figure 2. Double-ternary diagram of the relative abundances of the C_{28} 1,13-diol, C_{30} 1,13-diol, C_{30} 1,15-diol, and C_{32} 1,15-diol from LdRS short core (LdRS shc ~ 200 years) and LdRS long core (LdRS lgc ~ 1500 years). Diol data compiled from the literature: lake sediments (Rampen et al., 2014a), algal cultures (Rampen et al., 2014a), marine sediments (de Bar et al., 2016; Lattaud et al., 2017a; Rampen et al., 2012, 2014b), river sediments/inputs (de Bar et al., 2016; Lattaud et al., 2017b), and river particulate organic matter (Lattaud et al., 2018a).

The different diol isomers in LdRS also show good agreement with the general temperature trends for southwestern Europe during the last ~ 1500 years (Abrantes et al., 2005; Luterbacher et al., 2016; Nieto-Moreno et al., 2013; Sicre et al., 2016, among others). The C_{30} and C_{32} 1,15-diols depict a positive relationship with temperatures, whereas the C_{28} and C_{30} 1,13-diols display a negative one. Thus, the LDI record obtained from the C_{28} and C_{30} 1,13-diols and the C_{30} 1,15-diol also show important fluctuations during the last ~ 1500 years, in agreement with the general temperature trends of the Common Era (CE). More specifically, LDI values in the LdRS lgc range from ~ 0.23 to 0.05 from ~ 400 to 1900 CE, with maximum and minimum values recorded at ~ 930 and ~ 1690 CE, respectively (Fig. 3). These changes are coeval with the minimum temperatures of the LIA and the maximum temperatures of the Medieval Climate Anomaly (MCA) in Europe (e.g., Luterbacher et al., 2016; Nieto-

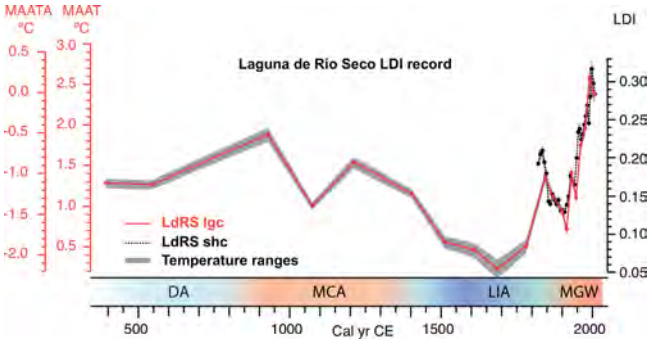

Figure 3. LDI record from LdRS, including both long core (solid line) and short core (dashed line), mean annual air temperature (MAAT, °C) reconstruction from LDI records of LdRS, and mean annual air temperature anomaly reconstruction (MAATA, °C) with respect to the annual MAAT of the last 30 years (1979–2008). The gray shading shows the reconstructed maximum and minimum temperature ranges obtained from the four LDI individual calibrations.

Moreno et al., 2013; Sicre et al., 2016). The rates of change were higher during the 20th century, with LDI values ranging from 0.10 to 0.31 in the lowest resolution LdRS lgc record and from 0.13 to 0.32 in the highest resolution LdRS shc record. These minimum and maximum values were reached in both cases during the first and last decades of the 20th century, respectively (Fig. 3).

3.2 LCD temperature calibration

A total of 26 samples from both short and long LdRS cores ranging in age from 1908 to 2008 were selected to perform the LCD-based temperature calibration, along with the two groups of reference temperature time series at 3020 m a.s.l. Since sedimentary samples used in the calibration have a time averaging period between 5 and 7 years, a mean of the historical temperatures covering the same time averaging period of each sample was calculated.

Eight different calibrations have been performed: five using the LDI; one using a multiple linear regression (MLR) of the relative abundances of the C_{28} 1,13-diol, C_{30} 1,13-diol, and C_{30} 1,15-diol (following Rampen et al., 2014a) (MLR calibration 1 hereafter); one using multiple linear regressions of the ratios of the relative abundances of LCDs with positive (even weak) correlation with temperature against the ones with negative correlation (C_{30} 1,15-/C_{28} 1,13-diols; C_{30} 1,15-/C_{30} 1,13-diols; C_{32} 1,15-/C_{28} 1,13-diols; and C_{32} 1,15-/C_{30} 1,13-diols) (MLR calibration 2 hereafter); and one using multiple linear regressions of the ratios of the relative abundances of the C_{30} 1,15-/C_{28} 1,13-diols and C_{30} 1,15-/C_{30} 1,13-diols (MLR calibration 3 hereafter). The statistics and the equations for the MLR calibrations 1, 2, and 3 are described in Table S8.

In the case of the LDI, ordinary least square regressions were run between the four reference temperature time series at 3020 m a.s.l. and the LDI record from LdRS shc and lgc, resulting in four calibration equations (Fig. S3). The slopes of these four equations range from 8.2 to 10.2. The LDI-derived temperatures from the reference time series 2 show the highest values for the last ∼ 100 years, whereas the minimum values are mainly shown by the ones calculated with the reference time series 1. The difference between the four LDI-derived temperatures for the last ∼ 100 years is low, with a standard deviation lower than 0.13. The standard error of these four individual calibrations ranges from 0.18 to 0.23 °C, and the maximum residual is ∼ 0.8 °C. However, due to the uncertainty of establishing an accurate temperature time series at 3020 m a.s.l., LDI-derived temperature values from these LDI individual calibrations have been used to determine the range of the variation (minimum and maximum temperature values) for each point, and an additional calibration, summarizing the relationship between LDI and the four reference temperatures at 3020 m a.s.l., has been performed. The obtained 104 combinations of LDI and temperature data provided an equation representing the average relationship between MAAT and LDI (Eq. 2; Fig. 4a). Since this is a summary of the four temperature time series, the residual errors include the residual errors of the individual LDI calibrations (Fig. S3). The residual errors of this average temperature calibration, according to both the LDI-reconstructed temperatures and the reference temperature time series, are lower than 0.8 °C (similar to the four individual LDI calibrations), with a standard error of 0.28 °C. The histogram showing the frequency of the residuals reveals that ∼ 85 % of the residuals range from 0.4 to −0.4 °C. This percentage is slightly lower (∼ 62 %) when the residual interval is established between 0.2 and −0.2 °C (Fig. 4b). Only one data point from 1973 among the 104 data combinations may be an outlier since it shows a residual 2.5 times higher than the residual standard deviation.

$$\text{MAAT } (^{\circ}\text{C}) = 9.147 \times \text{LDI} - 0.243$$
$$(n = 26 \times 4;\ r^2 = 0.79)^{*} \quad (2)$$

$^{*}n = 26$ LDI values plotted against four reference temperature time series providing a total of 104 combinations.

All the calibrations (LDI and MLR calibrations 1, 2, and 3) show good correlations with temperatures (Fig. 4 for LDI and Table S8 for MLR calibrations 1, 2, and 3). The obtained temperatures from the average LDI calibration and those using multiple linear regressions depict very similar trends in both cores (Fig. S4; $r > 0.96$; $p < 0.0001$). Nevertheless, the correlation is slightly weaker ($r > 0.82$; $p < 0.0001$) for the results from MLR calibration 1 in the long core. In addition, some inconsistencies come up in the reconstructed temperatures from MLR calibration 1: in general, temperatures tend to be lower than those from the other calibrations, giving rise to negative annual values during the LIA. This would be highly unlikely since under this scenario the lake would have

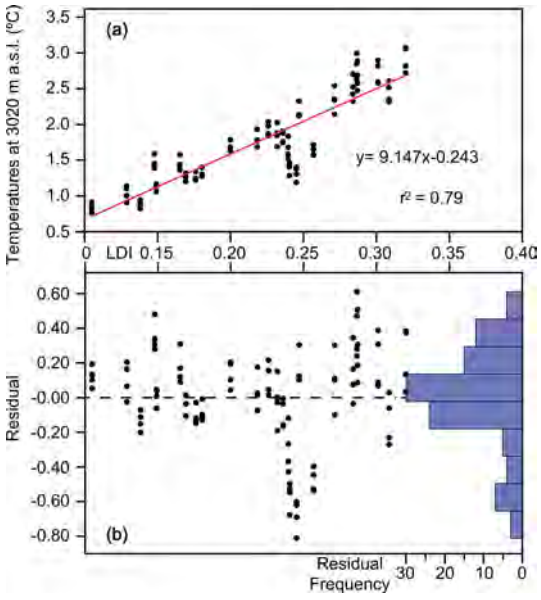

Figure 4. LDI temperature calibration. **(a)** Correlation by means of ordinary least square regression between both LDI records from LdRS (from 1908 to 2008) and the four reference temperature time series at 3020 m a.s.l. **(b)** LDI values of LdRS vs. residual temperatures (calculated between the calibrated LDI temperatures vs. reference temperature time series at 3020 m a.s.l.), as well as the histogram of the frequency of these residuals.

stayed frozen all year round, with little or no sedimentation occurring. Temperature reconstructions using MLR calibrations 2 and 3 take the advantage of the ratios of isomers with positive vs. negative relationships with temperatures. The results are similar to the ones obtained with the LDI, except for the LIA. Nevertheless, we discarded MLR calibration 2 as it also uses the C_{32} 1,15-diol, whose relationship with temperature is not clear, only reporting a positive correlation in some culture studies (Rampen et al., 2014b). MLR calibration 3 provides the most similar results to those from the LDI, especially comparing the temperature anomalies of both records with respect to the last 30 years of the record, showing differences of less than $\sim 0.1\,^{\circ}C$. However, this difference increases ($\sim 0.3\,^{\circ}C$) in the LIA. As this is the first study of LDI in sedimentary records from alpine lakes of the Sierra Nevada area, we have opted for a conservative solution following the LDI temperature calibration. The temperature reconstructions from MLR calibrations 1, 2, and 3 will only be mentioned when needed in the discussion.

The application of the obtained calibration to the LDI values of LdRS (Eq. 2) produced the first temperature reconstruction for the Common Era in this alpine area (Fig. 3). Nevertheless, a potential challenge of using this kind of downcore proxy calibrations is that the uncertainty of the reconstructed variables (temperature in this case) would increase when data fall outside the calibration data set (e.g., during the LIA). Further studies on the local LCD production in this alpine area will contribute to extend the range of temperatures in the calibration, reducing the uncertainties of the LCD-derived temperatures.

In order to estimate the real magnitude of temperature variations during the Common Era, the mean annual air temperature anomaly (MAATA, °C) has been calculated with reference to the annual MAAT of the last 30 years of the record (2008–1979). The lowest temperatures were recorded between ~ 1600 and ~ 1780 CE, with a temperature anomaly ranging from ~ -1.9 to $\sim -2.2\,^{\circ}C$. These temperature anomalies only reached positive values after 1998 (Fig. 3).

4 Discussion

4.1 Long-chain diol distribution in alpine lakes from southern Iberia

The distribution pattern of the main LCDs in LdRS (C_{28}, C_{30} 1,13- and C_{30}, C_{32} 1,15-diols) could help us decipher the potential biological producers. There is a high percentage of the C_{32} 1,15-diol, which is one of the main features observed in freshwater environments (Lattaud et al., 2018a; Rampen et al., 2014a) (Figs. 2, S5). Another relevant feature of the distribution of the LCDs in LdRS is the low and constant relative abundance of the C_{30} 1,15-diol ($6.5 \pm 1.5\,\%$) throughout the LdRS records (Fig. 2), agreeing with the range of the most probable distribution of the C_{30} 1,15-diol in marine algae (Fig. S5; Table S9). This feature is not common in marine or lake sediments (de Bar et al., 2016; Lattaud et al., 2017a; Rampen et al., 2014a), resulting in an almost unique area for LdRS isomers (most specifically C_{28} 1,13-, C_{30} 1,15-, and C_{32} 1,15-diols) when comparing with literature data in a ternary diagram (Fig. 2). Conversely, the distribution of both C_{28} and C_{30} 1,13-diols usually shows similar patterns as other freshwater samples (Lattaud et al., 2018a; Rampen et al., 2014a) (Figs. 2, S5, Table S9). A Kruskal–Wallis ANOVA test was used to assess whether the distribution of the main LCDs in LdRS and from other sources (e.g., marine, freshwater, algal culture) were statistically different. Results point towards no significant differences between the whole LCD distribution in LdRS and the other sources. Nevertheless, the Kruskal–Wallis test found significant differences among individual isomers of the different sources (including LdRS). Subsequently, a Mann–Whitney U test was performed to compare pairs of groups (individual isomers from LdRS vs. individual isomers from source 1, 2, and so on), finding significant differences among most of them (Table S9). All these pieces of evidence suggest that the LCD distribution in the LdRS might differ from those of previous studies published to date, and the potential biological producers at LdRS would be thus uncertain.

Eustigmatophyceae algae (i.e. *Vischeria* sp., *Eustigmatos* sp.) have been commonly proposed as the main diol producers in freshwater environments dominated by a mix of

the C_{28} 1,13-, C_{30} 1,15-, and C_{32} 1,15-diols (Rampen et al., 2014a; Villanueva et al., 2014; Volkman et al., 1999). Moreover, a dominance of the C_{32} 1,15-diol has been identified in families of Goniochloridaceae and Monodopsidaceae (Lattaud et al., 2018a; Rampen et al., 2014a). Nevertheless, planktonic algae communities are very simple in the alpine Sierra Nevada wetlands (Sánchez-Castillo, 1988) and Eustigmatophyceae algae have not been identified so far (Barea-Arco et al., 2001; Sánchez-Castillo, 1988). Thus, this study suggests that LCD producers in LdRS might be different from those identified previously in other freshwater environments and algal culture studies, making the potential source of LCDs even more complex than originally thought. Consequently, the outcomes of this paper (i.e., the LCD-based temperature calibration) should not be generally applied to other freshwater records unless they show a similar LCD distribution as LdRS. Additional research combining lipids and 18S rRNA (ribosomal RNA) gene sequencing analyses from suspended particulate matter, surface sediments, and sediment traps would be needed to unravel the real biological sources of LCDs in these alpine wetlands.

4.2 LdRS records in the environmental context of the Iberian Peninsula during the Common Era

Abrupt changes in temperature and precipitation have been depicted during the last 2000 years in the Iberian Peninsula and surrounding marine areas (Moreno et al., 2012; Sánchez-López et al., 2016). Precipitation was highly variable, showing arid conditions during the MCA, especially in southern Iberia, overall humid conditions throughout the LIA (with a complex internal structure showing large variability in humidity and extreme events), and arid conditions for the industrial period (Moreno et al., 2012; Oliva et al., 2018; Rodrigo et al., 1999; Sánchez-López et al., 2016), especially in high-elevation wetlands from southern Iberia (Anderson et al., 2011; Garcia-Alix et al., 2017; Jiménez-Espejo et al., 2014).

Although the Early Middle Ages displayed a great temperature variability in the Iberian Peninsula and surrounding marine sites (Moreno et al., 2012; Sánchez-López et al., 2016), three main stages have been identified for the last millennium deduced from different proxies: a warm period throughout the MCA followed by cold temperatures during the LIA, ending in an abrupt warming in the second half of the 20th century (Moreno et al., 2012; Oliva et al., 2018; Sánchez-López et al., 2016). One of the proxies used to reconstruct such temperature variations in continental areas of the Iberian Peninsula has been tree-ring data. Long tree-ring temperature archives of the Iberian Peninsula showed the same overall variations as the ones registered in LdRS, such as high temperatures before 1250 CE (Büntgen et al., 2017), some temperature declines coeval with solar minima during the LIA (e.g., the end of Spörer or Maunder Minimum), and a period of moderate-to-low temperatures from $\sim$ 1850 to $\sim$ 1940, followed by an increasing temperature trend in the second half of the 20th century with several temperature drops between $\sim$ 1960 and $\sim$ 1990 (Büntgen et al., 2017; Tejedor et al., 2017). Nevertheless, the warming documented from the LCD-derived temperatures in the last stages of the LIA is more pronounced in the LdRS record. The same overall trends have been observed in European summer temperatures deduced from tree-ring records (Luterbacher et al., 2016) (Figs. 5b, d, and 6b, c). Surprisingly, tree-ring data from the Pyrenees and other Iberian areas show minor temperature variations and even a slight temperature decrease from $\sim$ 2000 to 2008 similar to the one observed in the LCD-derived temperatures from the LdRS record (Fig. 4c). This temperature stabilization at the beginning of the 21st century is coeval with globally reduced warming rates over the 2001–2014 period (Fyfe et al., 2016).

Contrasting with these continental temperature reconstructions, high-resolution sea surface temperature (SST) estimations from marine sites surrounding the Iberian Peninsula, such as those derived from alkenones ($U^{K'}_{37}$) in the Tagus delta (Iberian Atlantic margin) or in the Balearic Islands (western Mediterranean Sea), showed a general decreasing trend for the last $\sim$ 2000 years, with a warm MCA, a cold LIA, and cold-to-moderate temperatures for the industrial period that do not appear to mirror the modern global warming observed throughout the 20th century (Abrantes et al., 2005; Moreno et al., 2012). Only high-resolution $U^{K'}_{37}$- and TEX_{86}-derived (from GDGTs) SST records of the cores 384B and 436B from the Alboran Sea (Nieto-Moreno et al., 2013) and the $U^{K'}_{37}$-SST record of core Gol-Ho1B from the Gulf of Lion (Sicre et al., 2016) have shown a clear temperature increase during the 20th century, similar to the LDI temperature record in LdRS (Figs. 5a, d, 6a, c). The observed heterogeneity in the SST reconstructions based on different biomarkers such as alkenones (Abrantes et al., 2005; Moreno et al., 2012; Rodrigo-Gámiz et al., 2014), GDGTs (Nieto-Moreno et al., 2013), or LCDs (Rodrigo-Gámiz et al., 2014) could be explained since each record belongs to a different biogeographical area influenced by specific temporal and dynamic oceanographic regimes, as well as by different primary productivity patterns of each biological source (e.g., seasonality or bloom length) (Sicre et al., 2016).

The previously described climate variability in precipitation and temperature during the last $\sim$ 1500 years in the Iberian Peninsula has been explained by different forcing mechanisms such as the effect of the westerlies–North Atlantic climate dynamics, internal climate variability, solar irradiance, volcanism, or anthropogenic forcing (Gómez-Navarro et al., 2011, 2012; Moreno et al., 2012; Sánchez-López et al., 2016). Their potential effect on the LCD distribution in the LdRS records is discussed in the following section.

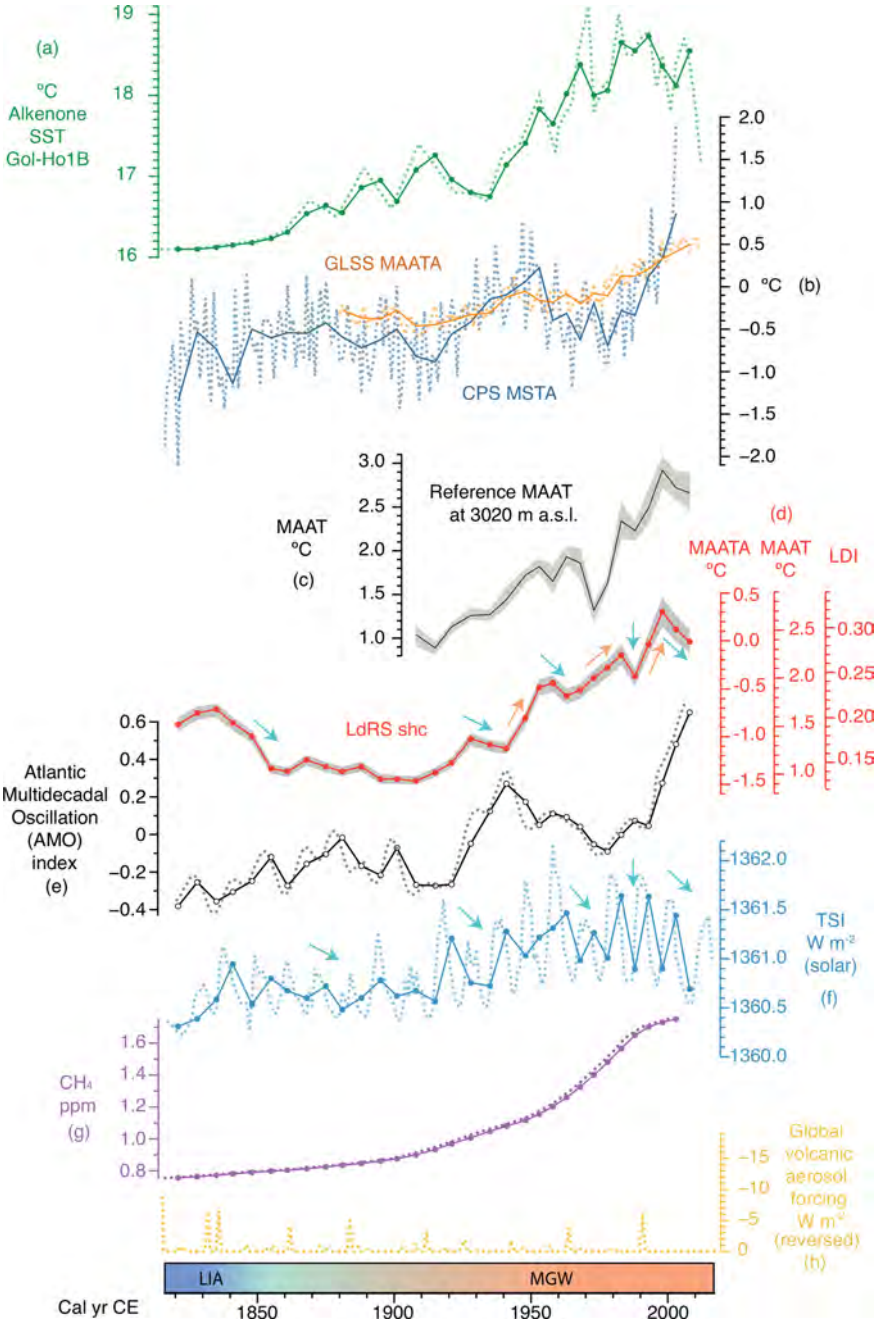

Figure 5. Comparison of the LDI record and the reconstructed temperatures for the last ∼ 200 years of LdRS with marine and terrestrial temperature records, Atlantic multidecadal oscillations, greenhouse gases, solar radiation, and volcanic eruption records. Original data are shown by dashed lines. Solid lines represent the same time averaging as the LDI data in LdRS shc (data were linearly interpolated and time averaged to the same resolution as the sampling points of LdRS shc) to facilitate the correlation. **(a)** Alkenone-derived sea surface temperatures (SST, °C) of the core Gol-Ho1B_KSGC-31 (Gulf of Lion: NW Mediterranean Sea; Sicre et al., 2016). **(b)** Composite-plus-scaling (CPS) mean summer temperature anomaly reconstruction from tree-ring records in Europe with respect to 1974–2003 (MSTA, °C) (Luterbacher et al., 2016) as well as global land and sea surface (GLSS) mean annual temperature anomalies with respect to 1979–2008 CE (MAATA, °C) (Hansen et al., 2010). **(c)** Summary of the four reference temperature time series at 3020 m a.s.l.: gray shading shows the maximum and minimum temperature ranges, and the black solid line represents the mean temperature values; **(d)** LDI record along with the reconstructed mean annual air temperatures (MAAT, °C) and mean annual air temperature anomalies with respect to 1979–2008 CE (MAATA, °C) for the last ∼ 200 years in LdRS; **(e)** Atlantic Multidecadal Oscillation (AMO) reconstruction (Mann et al., 2009); **(f)** high-resolution total solar irradiance reconstruction (TSI, W m^{-2}) (Coddington et al., 2016); **(g)** reconstructed concentration of atmospheric CH_4 (ppm) (Schmidt et al., 2011); and **(h)** reconstruction of the global volcanic aerosol forcing (W m^{-2}) (reversed) (Sigl et al., 2015). Acronyms: LIA, Little Ice Age; MGW, modern global warming. Blue arrows: decrease; orange arrows: increase.

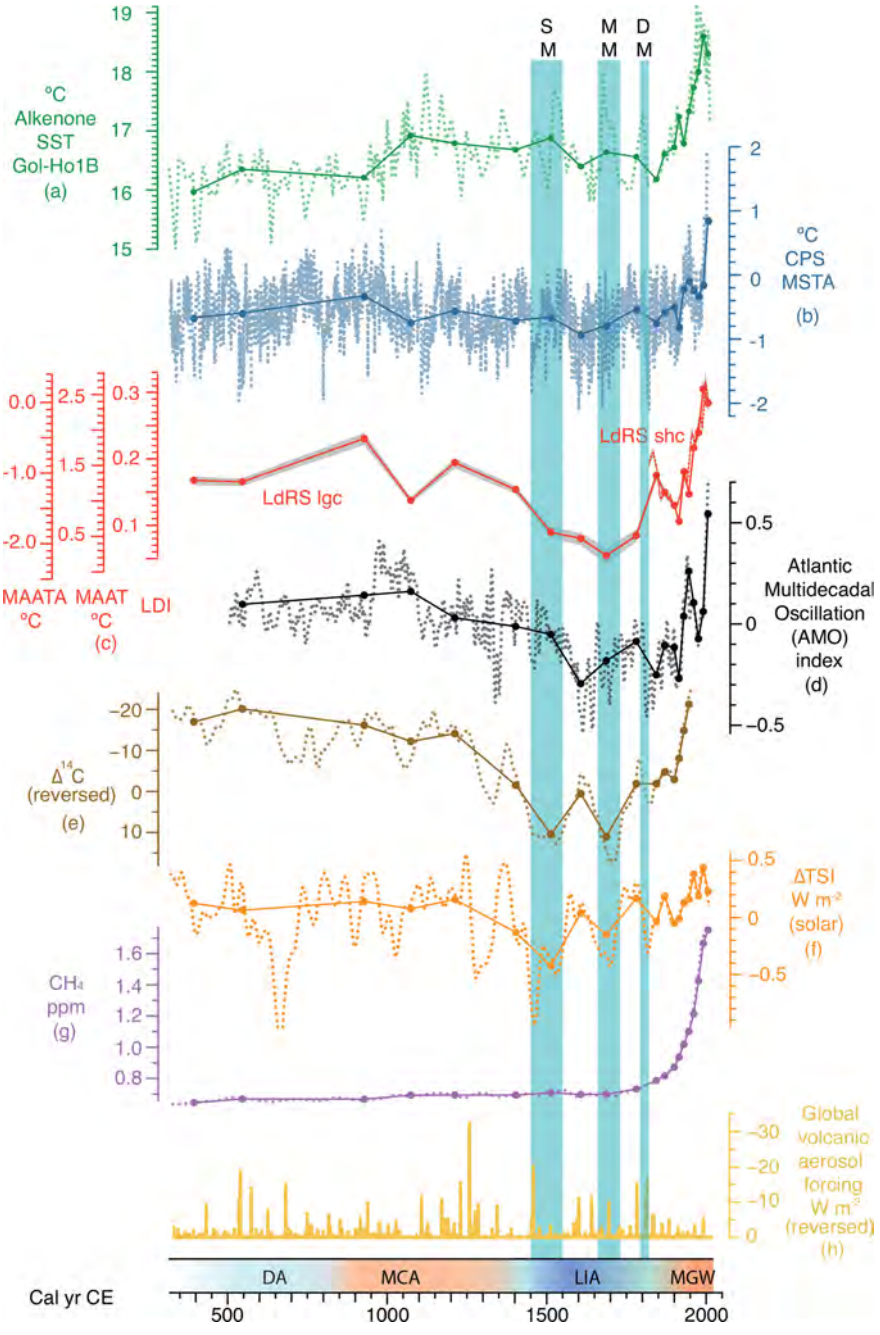

Figure 6. Comparison of the LDI record and the reconstructed temperatures for the last ∼ 1500 years of LdRS with marine and terrestrial temperature records, Atlantic multidecadal oscillations, solar radiation, greenhouse gases, and volcanic eruption records. Original data are shown by dashed lines. Solid dots represent the same time averaging as the LDI data in LdRS lgc (data were linearly interpolated and time averaged to the same resolution as the sampling points of LdRS lgc) to facilitate the Pearson correlation: **(a)** alkenone sea surface temperatures (SST, °C) of the core Gol-Ho1B_KSGC-31 (Gulf of Lion: NW Mediterranean Sea; Sicre et al., 2016). **(b)** Composite-plus-scaling (CPS) mean summer temperature anomaly reconstruction from tree-ring records in Europe with respect to 1974–2003 CE (MSTA, °C) (Luterbacher et al., 2016). **(c)** LDI record along with the reconstructed mean annual air temperatures (MAAT, °C) and mean annual air temperature anomalies with respect to 1979–2008 CE (MAATA, °C) for the last 1500 years in LdRS; **(d)** Atlantic Multidecadal Oscillation (AMO) reconstruction (Mann et al., 2009); **(e)** $\Delta^{14}C$ in the atmosphere (reversed) (Reimer et al., 2013); **(f)** reconstruction of the difference of the total solar irradiance from the value of the PMOD composite series during the solar cycle minimum of the year 1986 CE (1365.57 W m^{-2}) (ΔTSI) (Steinhilber et al., 2009); **(g)** reconstructed concentration of atmospheric CH_4 (ppm) (Schmidt et al., 2011); and **(h)** reconstruction of the global volcanic aerosol forcing (W m^{-2}) (reversed) (Sigl et al., 2015). Acronyms: DA, dark ages; MCA, Medieval Climate Anomaly; LIA, Little Ice Age; MGW, modern global warming. Blue bars show three low-solar-activity periods, the Spörer Minimum (SM), the Maunder Minimum (MM), and the Dalton Minimum (DM).

4.3 Control mechanisms on alpine temperatures in SW Europe during the Common Era

This discussion is based on the LDI-temperature reconstruction. However, similar results are obtained when comparing the temperature reconstructions from MLR calibrations 1, 2, and 3 in LdRS and the different forcing mechanisms assessed in this section (Tables S10–S13).

Solar, volcanic, and anthropogenic (e.g., CO_2 and CH_4) radiative changes, along with the internal variability, are usually attributed as the leading factors controlling temperatures during the Common Era (Ammann et al., 2007; IPCC, 2013). In addition, North Atlantic climate dynamics such as the North Atlantic Oscillation (NAO) or the Atlantic Multidecadal Oscillation (AMO) are other potential drivers of natural climate variability in the Iberian Peninsula (López-Moreno et al., 2011; Moreno et al., 2012; O'Reilly et al., 2017; Sánchez-López et al., 2016). The control of the North Atlantic climate dynamics in the studied alpine wetlands is evident, at least for precipitation and humidity fluctuations, since the NAO and solar forcing have been described as the main controls on the paleoenvironmental evolution recorded in this area (Garcia-Alix et al., 2017; Ramos-Román et al., 2016). Conversely, other studies have shown that the NAO climate mode had little effect on temperatures in this alpine area from 1950 to 2006 CE (López-Moreno et al., 2011). LdRS data agree with this observation, since no correlation (Tables S10–S13) has been detected between the NAO reconstruction (Trouet et al., 2009) and the obtained LCD record for the last millennium. The AMO has an impact on the North Atlantic atmospheric blocking mechanisms (Häkkinen et al., 2011) and on the European and Mediterranean temperatures, especially during the AMO warm phases (O'Reilly et al., 2017). In the study area, the AMO shows a moderate long-term correlation (Figs. 5d, e and 6c, d; $r > 0.60$; $p < 0.01$) with both long and short core LDI-derived records, but the correlation decreases when long-term trends are removed ($r < 0.32$; $p > 0.1$) (Tables S10, S11). Since the nature of the AMO and its specific drivers are still a matter of debate, i.e., internal ocean variability control (multidecadal fluctuations in the Atlantic Meridional Overturning Circulation) versus solar or volcanic forcing for the last centuries (Knudsen et al., 2014), we cannot conclude whether the observed correlations represent the sole effect of the AMO or the influence of its underlying forcing mechanisms.

The significant correlation at long and short terms ($r > 0.61$; $p < 0.005$) between LDI-derived temperatures from the LdRS records and greenhouse gases (Schmidt et al., 2011) (Fig. 6c, g; Table S10), especially since the beginning of the 20th century (industrial period) (Fig. 5d, g; Table S11), suggests that greenhouse gases might have an important effect on temperatures at this high-elevation site.

The potential impact of solar radiation and volcanic eruptions on climate over both short and long timescales is a topic of controversy in the literature (Ammann et al., 2007). In this regard, volcanic forcing, which should give rise to negative radiative forcing in the climate system (Ammann et al., 2007; Sigl et al., 2015), does not show a significant correlation with LDI-derived temperatures from the LdRS records over the last 1500 years (Figs. 5d, h and 6c, h; Tables S10, S11). We suggest that this lack of influence on LdRS records is a function of its high-altitude location, at 3020 m a.s.l., in the free troposphere, which reduces the environmental impact of small volcanic tropospheric eruptions that likely have greater effects on lower-elevation sites (Mather et al., 2013). In addition, the relatively short residence time of volcanic aerosols in the atmosphere mainly causes, at most, decadal effects (Sigl et al., 2015) that can be difficult to identify in most sedimentary records due to the age resolution, as in the case of sediments older than 200 years in LdRS. Nevertheless, large explosive volcanic eruptions delivering large amounts of stratospheric aerosols (Marotzke and Forster, 2015; Sigl et al., 2015), such as that for Agung Volcano in Bali, Indonesia (1963–1964 CE), may be associated with a small depression in LDI-derived temperatures observed in the LdRS records (Fig. 5d, h). Although cold LDI-reconstructed temperatures occasionally seem to occur coevally with volcanic eruptions, e.g., 560–510 and 320 years ago ($\sim$ 1450–1500 and 1690 CE) (Sigl et al., 2015), there is no consistent relationship between the intensity or number of large eruptions and the reconstructed coolings in the LdRS records, especially over the last $\sim$ 200 years when the sample resolution would be enough to detect them (LdRS shc).

Most of the abovementioned cooling events recorded in LdRS, such as those during the LIA, are coeval with low-solar-activity periods like the Spörer Minimum (from $\sim$ 1450 to 1550 CE) or the Maunder Minimum (from $\sim$ 1645 to 1715 CE) (Stuiver and Quay, 1980) (Fig. 6). Thus, long-term correlations between LDI-derived temperatures and solar activity, based on reconstructions of the solar irradiance and cosmogenic isotopes (such as ^{14}C), are evident during the last $\sim$ 1500 years in the LdRS record ($r > 0.69$; $p < 0.002$) (Fig. 6c, e, f; Table S11). This correlation drops ($0.37 < r < 0.56$ and $0.04 < p < 0.14$) when long-term trends are removed (Table S11). The long-term solar influence agrees with previous observations in other alpine records of this area (Garcia-Alix et al., 2017; Ramos-Román et al., 2016). Solar activity slightly decreases its long-term influence in the LdRS record during the last $\sim$ 200 years ($r > 0.56$; $p < 0.001$) and disappears when long-term trends are removed (Table S10). Only some occasional temperature decreases or slower rates of warming such as during the 19th to 20th century transition, from $\sim$ 1930 to 1940, from $\sim$ 1960 to 1975, and around 1988 CE, are coeval with slight declines in the total solar activity (Fig. 5d, f: blue arrows).

In the same way, LdRS registered a small decrease in LDI-derived temperatures (or stabilization) at the beginning of the 21st century (Fig. 5d), also recorded in the Madrid and Seville temperature time series (Spanish National Weather Agency – AEMet Open Data, 2019), and thus in the recon-

structed reference temperatures time series at 3020 m a.s.l. (Fig. 5c), in tree-ring records of the Pyrenees and Iberian Range (Büntgen et al., 2017; Tejedor et al., 2017), in marine platforms of the western Mediterranean (Fig. 5a) (Sicre et al., 2016), and globally (Fyfe et al., 2016). Although this slowdown agrees with a decreasing trend in solar activity and a slight stabilization of atmospheric methane concentrations (Fig. 5f, g), the causes are more complex and probably related to a combination of internal variability and radiative forcing (e.g., volcanic and solar activity or decadal changes in anthropogenic aerosols) (Fyfe et al., 2016).

4.4 Exceeding natural thresholds in alpine areas

The LDI-derived temperatures from LdRS exceeded the highest preindustrial temperatures in the early 1950s (Fig. 6c) under full anthropogenic influence. The comparison between preindustrial and postindustrial scenarios in the study site highlights the human impact on natural trends. In this regard, the temperature increase during the last stages of the LIA (from ∼ 1690 to ∼ 1850 CE), an analog for a non-anthropogenic temperature-increase scenario, was between ∼ 1.2 and ∼ 1.4 °C (∼ 0.09 °C per decade; Fig. 6), whereas the mean temperature rise throughout the 20th century was ∼ 1.8 °C (∼ 0.18 °C per decade; Fig. 7). Both warming rates are roughly similar to those reconstructed from MLR calibrations 1, 2, and 3: ∼ 0.06–0.09 °C per decade for the last stages of the LIA and ∼ 0.17–0.18 °C per decade for the 20th century. Although this means that, on average, the warming rate was 2 times faster throughout the 20th century than at the end of the LIA (Fig. 7), these observations are based on a low sample density for the LIA (8 samples), which might slightly increase the uncertainty for this period. By comparison, average global temperatures rose by ∼ 0.85 °C from 1880 to 2012 CE, corresponding to ≈ 0.06 °C per decade (IPCC, 2013), which highlights the amplification effect of high-elevation temperatures on this vulnerable area.

Other European alpine areas in the Mediterranean region, such as those from the Alps, experienced a slower warming rate during the 20th century (∼ 0.11 °C per decade) (Fig. 7) (Auer et al., 2007; Böhm et al., 2010). This is ∼ 1.6 times slower than the warming rate recorded in the Sierra Nevada. This evidence, along with the generally smaller amount of precipitation in the alpine areas of the western Mediterranean region (Auer et al., 2007; Rodrigo et al., 1999), allows us to conclude that the 20th century environmental stress in this area was greater than in the Alps.

Future scenarios are not optimistic for the Sierra Nevada since temperatures at ∼ 1000 m a.s.l. may rise between 2.2 and 5.3 °C by the end of the 21st century (Pérez-Luque et al., 2016), exceeding the global projections of the IPCC 2013 report (IPCC, 2013). However, temperature projection and its subsequent impact on alpine areas of the Sierra Nevada have not been satisfactorily assessed so far due to the lack of long-term quantitative climatic records at these

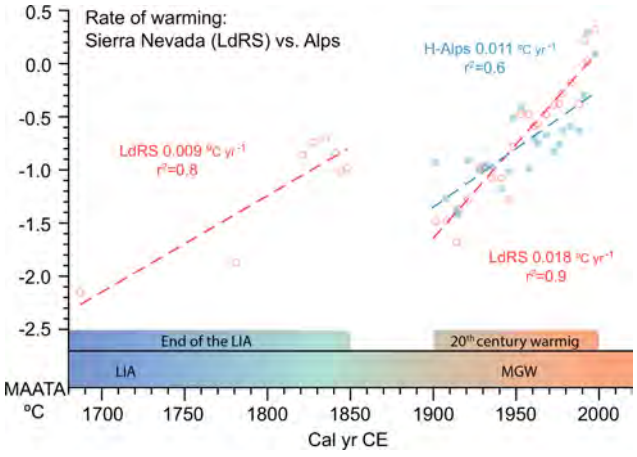

Figure 7. Comparison between the average temperature warming rates from LdRS and the alpine areas of the Alps by means of ordinary least square regressions. LDI-deduced MAATA (respect to the period 1979–2008 CE) from LdRS long and short cores for the last stage of the LIA and the 20th century (red open circles), and high-Alps historical (homogenized) temperature records from the Historical Instrumental Climatological Surface Time Series of the Greater Alpine Region (HISTALP) database (Auer et al., 2007; Böhm et al., 2010) at the same time averaging as LdRS shc and lgc to facilitate the comparison (blue closed squares).

elevations (e.g., temperature). LCD-based temperatures at ∼ 3000 m a.s.l. will solve this lack of quantitative data and will be valuable to project future scenarios in these alpine ecosystems, which are inhabited by endemic and endangered species (Blanca, 2001; Munguira and Martin, 1993).

4.5 Impact on the southwesternmost European alpine glaciers

The studied alpine area supported the southernmost glaciers in Europe during the LIA. Glaciers and permanent snow fields below ∼ 3000 m a.s.l., such as those of Corral del Mulhacen (∼ 2950 m a.s.l.) whose last mention in the literature was between 1809 and 1849 CE (Oliva and Gomez-Ortiz, 2012), would have totally disappeared by the decrease in regional precipitation during the first half of the 19th century (Rodrigo et al., 1999). The climatic features at the end of the 19th century and the beginning of the 20th century did not allow this glacier to re-establish itself (Fig. 8). Post-LIA climatic conditions have also been proposed as the trigger for the melting of the Corral del Veleta glacier in Sierra Nevada (∼ 3100 m a.s.l.) at the beginning of the 20th century (Garcia-Alix et al., 2017; Oliva and Gomez-Ortiz, 2012; Oliva et al., 2018). However, the LCDs in LdRS records show that reconstructed temperatures did not exceed the levels of the 1850s until the late 1940s. Precipitation was low in the southern Iberian Peninsula during the first half of the 20th century, but similar, and even lower, precipitation values were registered before ∼ 1850 CE (Rodrigo et al., 1999;

Spanish National Weather Agency – AEMet Open Data, 2019) (Fig. 8). Therefore, how could the glacier have retreated under this almost steady-state scenario? A similar paradox has been described in the Alps (Painter et al., 2013), where glaciers began to sharply retreat after the mid-19th century, even though temperature and precipitation records would suggest that glacier expansion should have occurred at least until the first decades of the 20th century. In this case, one of the proposed triggers for the glacier retreat was the industrial black carbon deposition that amplified the solar radiation absorbed at the snow surface and caused its subsequent melting – not a temperature or precipitation change (Painter et al., 2013). Precipitation data from southern Iberia (Rodrigo et al., 1999) along with the LCD-reconstructed temperatures in LdRS records suggest that temperature and precipitation were not the only drivers of glacial retreat that led to the melting of permanent glaciers in the Sierra Nevada in the 1920s. Instead, mirroring the case of the Alps, it is plausible that other factors reducing the albedo, such as enhanced atmospheric deposition, may have played a strong role. In this regard, important atmospheric depositional events have been recorded in the alpine study sites of southern Iberia from the mid-19th century to the first decades of the 20th century caused by both enhanced North African dust fluxes (Mulitza et al., 2010; Jiménez et al., 2018) as well as a spike in atmospheric pollution (as observed in anthropogenic Pb and Hg records in Sierra Nevada; Fig. 8) (Garcia-Alix et al., 2013, 2017). Similarly, both phenomena have been demonstrated as triggers for glacier retreat (Painter et al., 2013) and snow melt in the Alps (Di Mauro et al., 2019).

Melting of the last glaciated area in the Sierra Nevada during the first decades of the 20st century (Grunewald and Scheithauer, 2010) represents an important turning point regarding recent environmental change in this alpine region (Garcia-Alix et al., 2017; Jiménez et al., 2019). The rapid pace of environmental change in the area after this date is attributed to an amplified effect of warming and aridification (Fig. 8b, c) that increased stress on vulnerable ecosystems (Garcia-Alix et al., 2017; Jiménez et al., 2018, 2019) with little hope for return of local glaciers.

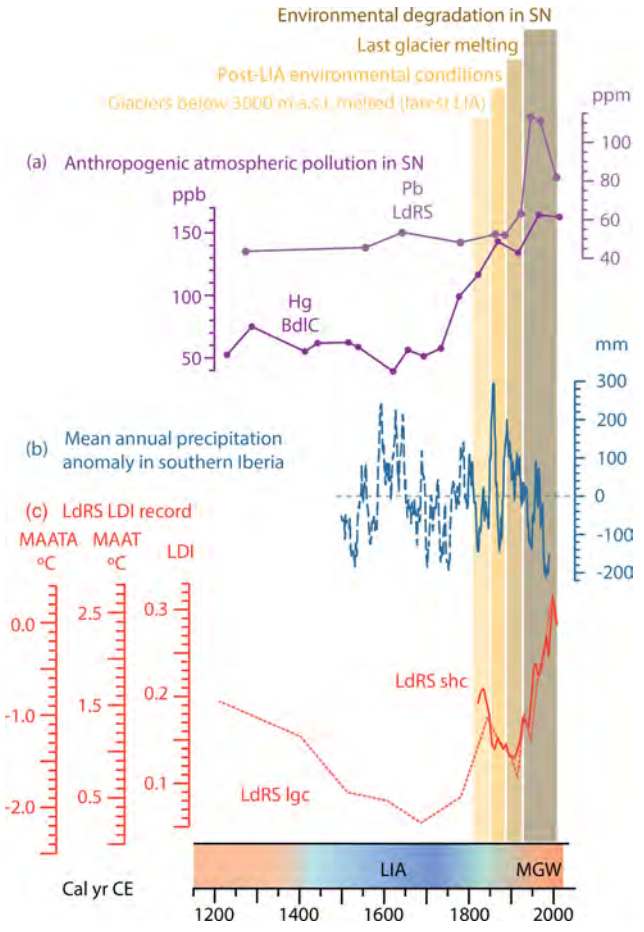

Figure 8. Comparison among different factors affecting the environmental evolution of alpine wetlands in the Sierra Nevada. **(a)** Records of anthropogenic heavy-metal atmospheric pollution (Pb and Hg) in two alpine sites of the Sierra Nevada: Laguna de Río Seco (LdRS) and Borreguil de la Caldera (BdlC) (Garcia-Alix et al., 2013, 2017); **(b)** mean annual precipitation anomaly in southern Iberia from 1500 to 1990 CE with respect to the mean value of the instrumental period (1791–1990 CE): solid line – instrumental data from Gibraltar (southern Iberia); dashed line – precipitation anomaly reconstruction (Rodrigo et al., 1999); **(c)** LDI and reconstructed temperatures in LdRS. Color bars indicate the four main environmental stages in the Sierra Nevada (SN) during the last 200 years. Acronyms: LIA, Little Ice Age; MGW, modern global warming.

5 Concluding remarks

This study shows the vulnerability of alpine regions and the importance of their monitoring for a better understanding of climate variability and future rapid responses. In this regard, algal-derived biomarkers from LdRS records have given rise to the first long-chain alkyl diol temperature calibration in freshwater environments by means of the comparison with instrumental temperature time series. The combination of both short and long sediment cores has provided both a highly accurate LCD-temperature calibration for the instrumental period and a long-term historical perspective on the modern warming. This approach delivers a better time-integrated temperature model than discrete temperature measurements for the 20th century. Nevertheless, the lack of information about the biological sources of LCDs in the Sierra Nevada means that this calibration can only be potentially applied to other lakes with a similar LCD distribution or in the same alpine area.

The low sample resolution in the longer core before ∼ 1500 CE precludes us from constraining the main natural controls on temperatures in this high-elevation site for the Common Era. However, the general trends support that the

presumed primary effect of greenhouse gases on temperatures reconstructed from algal lipids in this alpine region of southern Iberia is likely modulated by long-term solar forcing. In recent times, greenhouse gases seem to be the major temperature driver in this high-elevation site. Volcanic forcing appears to have little effect on reconstructed temperatures in this alpine area. The Atlantic Multidecadal Oscillation (AMO) has also been shown to have a long-term effect in the study area; however, due its complex nature, the real effect of the AMO on LCD-reconstructed temperatures in LdRS records cannot be fully constrained. In any case, the effect of the internal climate variability on local temperatures cannot be ruled out. LdRS records also highlight the potential impact that nonclimatic environmental drivers such as atmospheric dust and pollution deposition can exert on these remote alpine environments (e.g., glacier or snow melting).

Alpine temperatures of southern Iberia exceeded the highest scores reached during preindustrial times in the 1950s. This means that the rate of warming throughout the 20th century doubled that of the last stages of the LIA. Furthermore, this modern warming rate is higher in the Sierra Nevada than in the Alps, highlighting the important environmental stress in the Sierra Nevada ecosystems. In addition to the amplified effect of warming and aridification, the local environmental pressure may have enhanced throughout the 20th century due to the disappearance of perennial snow fields and the gradual reduction of the seasonal snow cover, affecting the local water availability. Future projections suggest that warming in this fragile alpine region will continue at similar rates or even higher than ones registered during the last century.

Data availability. Fractional abundances of the C_{28} 1,13-diol, C_{28} 1,14-diol, C_{30} 1,13-diol, C_{30} 1,14-diol, C_{30} 1,15-diol, and C_{32} 1,15-diol from the studied cores (LdRS shc and LdRS lgc), along with the four reference temperature time series at 3020 m a.s.l. from 1908 to 2008, are available online at: https://doi.org/10.1594/PANGAEA.911244 (García-Alix et al., 2020).

Supplement. The supplement related to this article is available online at: https://doi.org/10.5194/cp-16-245-2020-supplement.

Author contributions. The study was conceived by AG-A and JLT. CPM, LJ, GJM, and RSA recovered the sediment cores. AG-A analyzed the samples and processed the data. All co-authors discussed the data and equally contributed to the preparation of the article.

Competing interests. The authors declare that they have no conflict of interest.

Acknowledgements. We would like to thank Victoria Slaymark (University of Glasgow) for her help preparing and analyzing the organic and inorganic samples, as well as Francisco Javier Bonet García, Carlos González Hidalgo, and María Jesús Esteban Parra for providing the temperature time series from the Sierra Nevada and southern Spain. We also want to thank the editor, Erin McClymont, and two anonymous reviewers for their useful comments and suggestions that improved the article.

Financial support. This research has been supported by the Seventh Framework Programme (grant no. NAOSIPUK (623027)), the Ministerio de Economía y Competitividad, Secretaría de Estado de Investigación, Desarrollo e Innovación (grant no. CGL2017-85415-R), the Ministerio de Economía y Competitividad, Secretaría de Estado de Investigación, Desarrollo e Innovación (grant no. CGL2013-47038-R), the Ministerio de Economía y Competitividad, Secretaría de Estado de Investigación, Desarrollo e Innovación (grant no. CGL2011-23483), and the Consejería de Economía, Innovación, Ciencia y Empleo, Junta de Andalucía, Agencia de Innovación y Desarrollo de Andalucía (grant no. P11-RNM 7332). This research has also been supported by grant no. 87/2007 of the Organismo Autónomo Parques Nacionales (OAPN)-Ministerio de Medio Ambiente, the research group no. RNM-190 of the Plan Andaluz de Investigación, Desarrollo e Innovación (Junta de Andalucía), and the Ramón y Cajal Fellowship (fellowship no. RYC-2015-18966) of the Ministerio de Economía y Competitividad, Secretaría de Estado de Investigación, Desarrollo e Innovación.

Review statement. This paper was edited by Erin McClymont and reviewed by two anonymous referees.

References

Abrantes, F., Lebreiro, S., Rodrigues, T., Gil, I., Bartels-Jónsdóttir, H., Oliveira, P., Kissel, C., and Grimalt, J. O.: Shallow-marine sediment cores record climate variability and earthquake activity off Lisbon (Portugal) for the last 2000 years, Quaternary Sci. Rev., 24, 2477–2494, 2005.

Ammann, C. M., Joos, F., Schimel, D. S., Otto-Bliesner, B. L., and Tomas, R. A.: Solar influence on climate during the past millennium: Results from transient simulations with the NCAR Climate System Model, P. Natl. Acad. Sci. USA, 104, 3713–3718, 2007.

Anderson, R. S., Jiménez-Moreno, G., Carrión, J., and Pérez-Martinez, C.: Postglacial history of alpine vegetation, fire, and climate from Laguna de Río Seco, Sierra Nevada, southern Spain, Quaternary Sci. Rev., 30, 1615–1629, 2011.

Auer, I., Böhm, R., Jurkovic, A., Lipa, W., Orlik, A., Potzmann, R., Schöner, W., Ungersböck, M., Matulla, C., Briffa, K., Jones, P., Efthymiadis, D., Brunetti, M., Nanni, T., Maugeri, M., Mercalli, L., Mestre, O., Moisselin, J.-M., Begert, M., Müller-Westermeier, G., Kveton, V., Bochnicek, O., Stastny, P., Lapin, M., Szalai, S., Szentimrey, T., Cegnar, T., Dolinar, M., Gajic-Capka, M., Zaninovic, K., Majstorovic, Z., and Nieplova, E.: HISTALP – historical instrumental climatological surface time series of the Greater Alpine Region, Int. J. Climatol., 27, 17–46, 2007.

Balzano, S., Lattaud, J., Villanueva, L., Rampen, S. W., Brussaard, C. P. D., van Bleijswijk, J., Bale, N., Sinninghe Damsté, J. S., and Schouten, S.: A quest for the biological sources of long chain alkyl diols in the western tropical North Atlantic Ocean, Biogeosciences, 15, 5951–5968, https://doi.org/10.5194/bg-15-5951-2018, 2018.

Barea-Arco, J., Pérez-Martínez, C., and Morales-Baquero, R.: Evidence of a mutualistic relationship between an algal epibiont and its host, Daphnia pulicaria, Limnol. Oceanogr., 46, 871–881, 2001.

Blanca, G.: Flora amenazada y endémica de Sierra Nevada, Consejería de Medio Ambiente de la Junta de Andalucía and University of Granada, 2001.

Böhm, R., Jones, P. D., Hiebl, J., Frank, D., Brunetti, M., and Maugeri, M.: The early instrumental warm-bias: a solution for long central European temperature series 1760–2007, Climatic Change, 101, 41–67, 2010.

Büntgen, U., Krusic, P. J., Verstege, A., Sangüesa-Barreda, G., Wagner, S., Camarero, J. J., Ljungqvist, F. C., Zorita, E., Oppenheimer, C., Konter, O., Tegel, W., Gärtner, H., Cherubini, P., Reinig, F., and Esper, J.: New Tree-Ring Evidence from the Pyrenees Reveals Western Mediterranean Climate Variability since Medieval Times, J. Climate, 30, 5295–5318, 2017.

Carrillo, P., Cruz-Pizarro, L., and Sánchez Castillo, P. M.: Aportación al conocimiento del ciclo biológico de Chromulina nevadensis, Acta Botánica Malacitana, 16, 19–26, 1991.

Castañeda, I. S. and Schouten, S.: A review of molecular organic proxies for examining modern and ancient lacustrine environments, Quaternary Sci. Rev., 30, 2851–2891, 2011.

Castillo Martín, A.: Lagunas de Sierra Nevada, Editorial Universidad de Granada, Granada, 2009.

Catalan, J., Pla-Rabés, S., Wolfe, A. P., Smol, J. P., Rühland, K. M., Anderson, N. J., Kopáček, J., Stuchlík, E., Schmidt, R., Koinig, K. A., Camarero, L., Flower, R. J., Heiri, O., Kamenik, C., Korhola, A., Leavitt, P. R., Psenner, R., and Renberg, I.: Global change revealed by palaeolimnological records from remote lakes: a review, J. Paleolimnol., 49, 513–535, 2013.

Coddington, O., Lean, J. L., Pilewskie, P., Snow, M., and Lindholm, D.: A Solar Irradiance Climate Data Record, B. Am. Meteorol. Soc., 97, 1265–1282, 2016.

Colcord, D. E., Cadieux, S. B., Brassell, S. C., Castañeda, I. S., Pratt, L. M., and White, J. R.: Assessment of branched GDGTs as temperature proxies in sedimentary records from several small lakes in southwestern Greenland, Org. Geochem., 82, 33–41, 2015.

de Bar, M. W., Dorhout, D. J. C., Hopmans, E. C., Rampen, S. W., Sinninghe Damsté, J. S., and Schouten, S.: Constraints on the application of long chain diol proxies in the Iberian Atlantic margin, Org. Geochem., 101, 184–195, 2016.

Di Mauro, B., Garzonio, R., Rossini, M., Filippa, G., Pogliotti, P., Galvagno, M., Morra di Cella, U., Migliavacca, M., Baccolo, G., Clemenza, M., Delmonte, B., Maggi, V., Dumont, M., Tuzet, F., Lafaysse, M., Morin, S., Cremonese, E., and Colombo, R.: Saharan dust events in the European Alps: role in snowmelt and geochemical characterization, The Cryosphere, 13, 1147–1165, https://doi.org/10.5194/tc-13-1147-2019, 2019.

Easterling, D. R., Meehl, G. A., Parmesan, C., Changnon, S. A., Karl, T. R., and Mearns, L. O.: Climate Extremes: Observations, Modeling, and Impacts, Science, 289, 2068–2074, 2000.

Foster, L. C., Pearson, E. J., Juggins, S., Hodgson, D. A., Saunders, K. M., Verleyen, E., and Roberts, S. J.: Development of a regional glycerol dialkyl glycerol tetraether (GDGT)–temperature calibration for Antarctic and sub-Antarctic lakes, Earth Planet. Sc. Lett., 433, 370–379, 2016.

Fyfe, J. C., Meehl, G. A., England, M. H., Mann, M. E., Santer, B. D., Flato, G. M., Hawkins, E., Gillett, N. P., Xie, S.-P., Kosaka, Y., and Swart, N. C.: Making sense of the early-2000s warming slowdown, Nat. Clim. Change, 6, 224–228, https://doi.org/10.1038/nclimate2938, 2016.

Gal, J.-K., Kim, J.-H., and Shin, K.-H.: Distribution of long chain alkyl diols along a south-north transect of the northwestern Pacific region: Insights into a paleo sea surface nutrient proxy, Org. Geochem., 119, 80–90, 2018.

García-Alix, A., Jiménez-Moreno, G., Anderson, R. S., Jiménez Espejo, F. J., and Delgado Huertas, A.: Holocene environmental change in southern Spain deduced from the isotopic record of a high-elevation wetland in Sierra Nevada, J. Paleolimnol., 48, 471–484, 2012.

Garcia-Alix, A., Jimenez-Espejo, F. J., Lozano, J. A., Jimenez-Moreno, G., Martinez-Ruiz, F., Garcia Sanjuan, L., Aranda Jimenez, G., Garcia Alfonso, E., Ruiz-Puertas, G., and Anderson, R. S.: Anthropogenic impact and lead pollution throughout the Holocene in Southern Iberia, Sci. Total Environ., 449, 451–460, 2013.

Garcia-Alix, A., Jimenez Espejo, F. J., Toney, J. L., Jiménez-Moreno, G., Ramos-Román, M. J., Anderson, R. S., Ruano, P., Queralt, I., Delgado Huertas, A., and Kuroda, J.: Alpine bogs of southern Spain show human-induced environmental change superimposed on long-term natural variations, Sci. Rep., 7, 7439, https://doi.org/10.1038/s41598-017-07854-w, 2017.

García Montoro, C., Titos Martínez, M., and Casado Sánchez de Castilla, M.: Sierra Nevada. Una expedición al pico de Veleta desde los Baños de Lanjarón (1859), Universidad de Granada, Editorial Universidad de Granada, 2016.

Giorgi, F.: Climate change hot-spots, Geophys. Res. Lett., 33, L08707, https://doi.org/10.1029/2006GL025734, 2006.

Gómez-Navarro, J. J., Montávez, J. P., Jerez, S., Jiménez-Guerrero, P., Lorente-Plazas, R., González-Rouco, J. F., and Zorita, E.: A regional climate simulation over the Iberian Peninsula for the last millennium, Clim. Past, 7, 451–472, https://doi.org/10.5194/cp-7-451-2011, 2011.

Gómez-Navarro, J. J., Montávez, J. P., Jiménez-Guerrero, P., Jerez, S., Lorente-Plazas, R., González-Rouco, J. F., and Zorita, E.: Internal and external variability in regional simulations of the Iberian Peninsula climate over the last millennium, Clim. Past, 8, 25–36, https://doi.org/10.5194/cp-8-25-2012, 2012.

Gonzalez-Hidalgo, J. C., Peña-Angulo, D., Brunetti, M., and Cortesi, N.: MOTEDAS: a new monthly temperature database for mainland Spain and the trend in temperature (1951–2010), Int. J. Climatol., 35, 4444–4463, 2015.

Grunewald, K. and Scheithauer, J.: Europe's southernmost glaciers: response and adaptation to climate change, J. Glaciol., 56, 129–142, 2010.

Häkkinen, S., Rhines, P. B., and Worthen, D. L.: Atmospheric Blocking and Atlantic Multidecadal Ocean Variability, Science, 334, 655–659, 2011.

Hansen, J., Ruedy, R., Sato, M., and Lo, K.: Global Surface Temperature Change, Rev. Geophys., 48, RG4004, https://doi.org/10.1029/2010RG000345, 2010.

IPCC: Climate Change 2013: The Physical Science Basis. Contribution of Working Group I to the Fifth Assessment Report of the Intergovernmental Panel on Climate Change, Cambridge University Press, Cambridge, United Kingdom and New York, NY, USA, 2013.

Jiménez, L., Romero-Viana, L., Conde-Porcuna, J. M., and Pérez-Martínez, C.: Sedimentary photosynthetic pigments as indicators of climate and watershed perturbations in an alpine lake in southern Spain, Limniteca, 34, 439–454, 2015.

Jiménez, L., Rühland, K. M., Jeziorski, A., Smol, J. P., and Pérez-Martínez, C.: Climate change and Saharan dust drive recent cladoceran and primary production changes in remote alpine lakes of Sierra Nevada, Spain, Glob. Change Biol., 28, e139–e158, 2018.

Jiménez, L., Conde-Porcuna, J. M., García-Alix, A., Toney, J. L., Anderson, R. S., Heiri, O., and Pérez-Martínez, C.: Ecosystem Responses to Climate-Related Changes in a Mediterranean Alpine Environment Over the Last ∼ 180 Years, Ecosystems, 22, 563–577, 2019.

Jiménez-Espejo, F. J., García-Alix, A., Jiménez-Moreno, G., Rodrigo-Gámiz, M., Anderson, R. S., Rodríguez-Tovar, F. J., Martínez-Ruiz, F., Giralt, S., Delgado Huertas, A., and Pardo-Igúzquiza, E.: Saharan aeolian input and effective humidity variations over western Europe during the Holocene from a high altitude record, Chem. Geol., 374–375, 1–12, 2014.

Jiménez-Moreno, G. and Anderson, R. S.: Holocene vegetation and climate change recorded in alpine bog sediments from the Borreguiles de la Virgen, Sierra Nevada, southern Spain, Quaternary Res., 77, 44–53, 2012.

Jiménez-Moreno, G., García-Alix, A., Hernández-Corbalán, M. D., Anderson, R. S., and Delgado-Huertas, A.: Vegetation, fire, climate and human disturbance history in the southwestern Mediterranean area during the late Holocene, Quaternary Res., 79, 110–122, 2013.

Knudsen, M. F., Jacobsen, B. H., Seidenkrantz, M.-S., and Olsen, J.: Evidence for external forcing of the Atlantic Multidecadal Oscillation since termination of the Little Ice Age, Nat. Commun., 5, 3323, https://doi.org/10.1038/ncomms4323, 2014.

Lattaud, J., Dorhout, D., Schulz, H., Castañeda, I. S., Schefuß, E., Sinninghe Damsté, J. S., and Schouten, S.: The C32 alkane-1,15-diol as a proxy of late Quaternary riverine input in coastal margins, Clim. Past, 13, 1049–1061, https://doi.org/10.5194/cp-13-1049-2017, 2017a.

Lattaud, J., Kim, J.-H., De Jonge, C., Zell, C., Sinninghe Damsté, J. S., and Schouten, S.: The C32 alkane-1,15-diol as a tracer for riverine input in coastal seas, Geochim. Cosmochim. Ac., 202, 146–158, 2017b.

Lattaud, J., Kirkels, F., Peterse, F., Freymond, C. V., Eglinton, T. I., Hefter, J., Mollenhauer, G., Balzano, S., Villanueva, L., van der Meer, M. T. J., Hopmans, E. C., Sinninghe Damsté, J. S., and Schouten, S.: Long-chain diols in rivers: distribution and potential biological sources, Biogeosciences, 15, 4147–4161, https://doi.org/10.5194/bg-15-4147-2018, 2018a.

Lattaud, J., Lo, L., Huang, J.-J., Chou, Y.-M., Gorbarenko, S. A., Sinninghe Damsté, J. S., and Schouten, S.: A Comparison of Late Quaternary Organic Proxy-Based Paleotemperature Records of the Central Sea of Okhotsk, Paleoceanography and Paleoclimatology, 33, 732–744, 2018b.

Longo, W. M., Huang, Y., Yao, Y., Zhao, J., Giblin, A. E., Wang, X., Zech, R., Haberzettl, T., Jardillier, L., Toney, J., Liu, Z., Krivonogov, S., Kolpakova, M., Chu, G., D'Andrea, W. J., Harada, N., Nagashima, K., Sato, M., Yonenobu, H., Yamada, K., Gotanda, K., and Shinozuka, Y.: Widespread occurrence of distinct alkenones from Group I haptophytes in freshwater lakes: Implications for paleotemperature and paleoenvironmental reconstructions, Earth Planet. Sc. Lett., 492, 239–250, 2018.

López-Moreno, J. I., Vicente-Serrano, S. M., Morán-Tejeda, E., Lorenzo-Lacruz, J., Kenawy, A., and Beniston, M.: Effects of the North Atlantic Oscillation (NAO) on combined temperature and precipitation winter modes in the Mediterranean mountains: Observed relationships and projections for the 21st century, Global Planet. Change, 77, 62–76, 2011.

Luterbacher, J., Werner, J. P., Smerdon, J. E., Fernández-Donado, L., González-Rouco, F. J., Barriopedro, D., Ljungqvist, F. C., Büntgen, U., Zorita, E., Wagner, S., Esper, J., McCarroll, D., Toreti, A., Frank, D., Jungclaus, J. H., Barriendos, M., Bertolin, C., Bothe, O., Brázdil, R., Camuffo, D., Dobrovolný, P., Gagen, M., García-Bustamante, E., Ge, Q., Gómez-Navarro, J. J., Guiot, J., Hao, Z., Hegerl, G. C., Holmgren, K., Klimenko, V. V., Martín-Chivelet, J., Pfister, C., Roberts, N., Schindler, A., Schurer, A., Solomina, O., von Gunten, L., Wahl, E., Wanner, H., Wetter, O., Xoplaki, E., Yuan, N., Zanchettin, D., Zhang, H., and Zerefos, C.: European summer temperatures since Roman times, Environ. Res. Lett., 11, 024001, https://doi.org/10.1088/1748-9326/11/2/024001, 2016.

Mann, M. E., Zhang, Z., Rutherford, S., Bradley, R. S., Hughes, M. K., Shindell, D., Ammann, C., Faluvegi, G., and Ni, F.: Global Signatures and Dynamical Origins of the Little Ice Age and Medieval Climate Anomaly, Science, 326, 1256–1260, 2009.

Marotzke, J. and Forster, P. M.: Forcing, feedback and internal variability in global temperature trends, Nature, 517, 565–570, 2015.

Mather, T. A., Pyle, D. M., and Oppenheimer, C.: Tropospheric Volcanic Aerosol, in: Volcanism and the Earth's Atmosphere, American Geophysical Union, 2013.

Médail, F. and Quézel, P.: Biodiversity Hotspots in the Mediterranean Basin: Setting Global Conservation Priorities, Conserv. Biol., 13, 1510–1513, 1999.

Mesa-Fernández, J. M., Jiménez-Moreno, G., Rodrigo-Gámiz, M., García-Alix, A., Jiménez-Espejo, F. J., Martínez-Ruiz, F., Anderson, R. S., Camuera, J., and Ramos-Román, M. J.: Vegetation and geochemical responses to Holocene rapid climate change in the Sierra Nevada (southeastern Iberia): the Laguna Hondera record, Clim. Past, 14, 1687–1706, https://doi.org/10.5194/cp-14-1687-2018, 2018.

Morales-Baquero, R., Pulido-Villena, E., and Reche, I.: Atmospheric inputs of phosphorus and nitrogen to the southwest Mediterranean region: Biogeochemical responses of high mountain lakes, Limnol. Oceanogr. 51, 830–837, 2006.

Moreno, A., Pérez, A., Frigola, J., Nieto-Moreno, V., Rodrigo-Gámiz, M., Martrat, B., González-Sampériz, P., Morellón, M., Martín-Puertas, C., Corella, J. P., Belmonte, Á., Sancho, C., Cacho, I., Herrera, G., Canals, M., Grimalt, J. O., Jiménez-Espejo, F., Martínez-Ruiz, F., Vegas-Vilarrúbia, T., and Valero-Garcés, B. L.: The Medieval Climate Anomaly in the Iberian Peninsula re-

constructed from marine and lake records, Quaternary Sci. Rev., 43, 16–32, 2012.

Mulitza, S., Heslop, D., Pittauerova, D., Fischer, H. W., Meyer, I., Stuut, J.-B., Zabel, M., Mollenhauer, G., Collins, J. A., Kuhnert, H., and Schulz, M.: Increase in African dust flux at the onset of commercial agriculture in the Sahel region, Nature, 466, 226–228, 2010.

Munguira, M. L. and Martin, J.: The Sierra Nevada blue, Polyommatus golgus (Hiibner), in: Conserv. Biol. of Lycaenidae (Butterflies), edited by: New, T. R., IUCN, Gland, Switzerland, 1993.

Nieto-Moreno, V., Martínez-Ruiz, F., Willmott, V., García-Orellana, J., Masqué, P., and Sinninghe Damsté, J. S.: Climate conditions in the westernmost Mediterranean over the last two millennia: An integrated biomarker approach, Org. Geochem., 55, 1–10, 2013.

Observatorio del cambio global de Sierra Nevada: Linaria v1.0. iEcolab – Laboratorio de Ecología Terrestre – Universidad de Granada, available at: http://linaria.obsnev.es (last access: 19 December 2019), 2016.

Oliva, M. and Gomez-Ortiz, A.: Late-Holocene environmental dynamics and climate variability in a Mediterranean high mountain environment (Sierra Nevada, Spain) inferred from lake sediments and historical sources, Holocene, 22, 915–927, 2012.

Oliva, M., Ruiz-Fernández, J., Barriendos, M., Benito, G., Cuadrat, J. M., Domínguez-Castro, F., García-Ruiz, J. M., Giralt, S., Gómez-Ortiz, A., Hernández, A., López-Costas, O., López-Moreno, J. I., López-Sáez, J. A., Martínez-Cortizas, A., Moreno, A., Prohom, M., Saz, M. A., Serrano, E., Tejedor, E., Trigo, R., Valero-Garcés, B., and Vicente-Serrano, S. M.: The Little Ice Age in Iberian mountains, Earth-Sci. Rev., 177, 175–208, 2018.

O'Reilly, C. H., Woollings, T., and Zanna, L.: The Dynamical Influence of the Atlantic Multidecadal Oscillation on Continental Climate, J. Climate, 30, 7213–7230, 2017.

Painter, T. H., Flanner, M. G., Kaser, G., Marzeion, B., VanCuren, R. A., and Abdalati, W.: End of the Little Ice Age in the Alps forced by industrial black carbon, P. Natl. Acad. Sci. USA, 110, 15216–15221, 2013.

Pauli, H., Gottfried, M., Dullinger, S., Abdaladze, O., Akhalkatsi, M., Alonso, J. L. B., Coldea, G., Dick, J., Erschbamer, B., Calzado, R. F., Ghosn, D., Holten, J. I., Kanka, R., Kazakis, G., Kollár, J., Larsson, P., Moiseev, P., Moiseev, D., Molau, U., Mesa, J. M., Nagy, L., Pelino, G., Puşcaş, M., Rossi, G., Stanisci, A., Syverhuset, A. O., Theurillat, J.-P., Tomaselli, M., Unterluggauer, P., Villar, L., Vittoz, P., and Grabherr, G.: Recent Plant Diversity Changes on Europe's Mountain Summits, Science, 336, 353–355, 2012.

Pérez-Luque, A., Peìrez-Peìrez, R., Aspizua, R., MunÞoz, J., and Bonet, F.: Climate in Sierra Nevada: present and future, in: Change impacts in Sierra Nevada: challenges for conservation, edited by: Zamora, R., Peìrez-Luque, A., Bonet, F., Barea-Azcoìn, J., and Aspizua, R., Consejerìa de Medio Ambiente y Ordenacioìn del Territorio, Junta de Andalucìa, Andalucia, 2016.

Pulido-Villena, E., Reche, I., and Morales-Baquero, R.: Food web reliance on allochthonous carbon in two high mountain lakes with contrasting catchments: a stable isotope approach, Can. J. Fish. Aquat. Sci., 62, 2640–2648, 2005.

Ramos-Román, M. J., Jiménez-Moreno, G., R.S., A., García-Alix, A., Toney, J. L., Jiménez-Espejo, F. J., and Carrión, J. S.: Centennial-scale vegetation and North Atlantic Oscillation changes during the Late Holocene in the southern Iberia, Quaternary Sci. Rev., 143, 84–95, 2016.

Rampen, S. W., Schouten, S., Koning, E., Brummer, G.-J. A., and Sinninghe Damsté, J. S.: A 90 kyr upwelling record from the northwestern Indian Ocean using a novel long-chain diol index, Earth Planet. Sc. Lett., 276, 207–213, 2008.

Rampen, S. W., Willmott, V., Kim, J.-H., Uliana, E., Mollenhauer, G., Schefuß, E., Sinninghe Damsté, J. S., and Schouten, S.: Long chain 1,13- and 1,15-diols as a potential proxy for palaeotemperature reconstruction, Geochim. Cosmochim. Ac., 84, 204–216, 2012.

Rampen, S. W., Datema, M., Rodrigo-Gámiz, M., Schouten, S., Reichart, G.-J., and Sinninghe Damsté, J. S.: Sources and proxy potential of long chain alkyl diols in lacustrine environments, Geochim. Cosmochim. Ac., 144, 59–71, 2014a.

Rampen, S. W., Willmott, V., Kim, J.-H., Rodrigo-Gámiz, M., Uliana, E., Mollenhauer, G., Schefuß, E., Sinninghe Damsté, J. S., and Schouten, S.: Evaluation of long chain 1,14-alkyl diols in marine sediments as indicators for upwelling and temperature, Org. Geochem., 76, 39–47, 2014b.

Reche, I., Ortega-Retuerta, E., Romera, O., Pulido-Villena, E., Morales-Baquero, R., and Casamayor, E. O.: Effect of Saharan dust inputs on bacterial activity and community composition in Mediterranean lakes and reservoirs, Limnol. Oceanogr., 54, 869–879, 2009.

Reimer, P. J., Bard, E., Bayliss, A., Beck, J. W., Blackwell, P. G., Ramsey, C. B., Buck, C. E., Cheng, H., Edwards, R. L., Friedrich, M., Grootes, P. M., Guilderson, T. P., Haflidason, H., Hajdas, I., Hatté, C., Heaton, T. J., Hoffmann, D. L., Hogg, A. G., Hughen, K. A., Kaiser, K. F., Kromer, B., Manning, S. W., Niu, M., Reimer, R. W., Richards, D. A., Scott, E. M., Southon, J. R., Staff, R. A., Turney, C. S. M., and van der Plicht, J.: IntCal13 and Marine13 Radiocarbon Age Calibration Curves 0–50,000 Years cal BP, Radiocarbon, 55, 1869–1887, 2013.

Rodrigo, F. S., Esteban-Parra, M. J., Pozo-Vázquez, D., and Castro-Díez, Y.: A 500-year precipitation record in Southern Spain, Int. J. Climatol., 19, 1233–1253, 1999.

Rodrigo-Gámiz, M., Martínez-Ruiz, F., Rampen, S. W., Schouten, S., and Sinninghe Damsté, J. S.: Sea surface temperature variations in the western Mediterranean Sea over the last 20 kyr: A dual-organic proxy (UK'37 and LDI) approach, Paleoceanography, 29, 87–98, 2014.

Rodrigo-Gámiz, M., Rampen, S. W., de Haas, H., Baas, M., Schouten, S., and Sinninghe Damsté, J. S.: Constraints on the applicability of the organic temperature proxies $U^{K'}_{37}$, TEX_{86} and LDI in the subpolar region around Iceland, Biogeosciences, 12, 6573–6590, https://doi.org/10.5194/bg-12-6573-2015, 2015.

Romero-Viana, L., Kienel, U., and Sachse, D.: Lipid biomarker signatures in a hypersaline lake on Isabel Island (Eastern Pacific) as a proxy for past rainfall anomaly (1942–2006AD), Palaeogeogr. Palaeocl., 350–352, 49–61, 2012.

Sánchez-Castillo, P. M.: Algas de las lagunas de alta montaña de Sierra Nevada (Granada, España), Acta Botánica Malacitana, 13, 21–52, 1988.

Sánchez-López, G., Hernández, A., Pla-Rabes, S., Trigo, R. M., Toro, M., Granados, I., Sáez, A., Masqué, P., Pueyo, J. J., Rubio-Inglés, M. J., and Giralt, S.: Climate reconstruction for the last two millennia in central Iberia: The role of East Atlantic (EA),

North Atlantic Oscillation (NAO) and their interplay over the Iberian Peninsula, Quaternary Sci. Rev., 149, 135–150, 2016.

Schmidt, G. A., Jungclaus, J. H., Ammann, C. M., Bard, E., Braconnot, P., Crowley, T. J., Delaygue, G., Joos, F., Krivova, N. A., Muscheler, R., Otto-Bliesner, B. L., Pongratz, J., Shindell, D. T., Solanki, S. K., Steinhilber, F., and Vieira, L. E. A.: Climate forcing reconstructions for use in PMIP simulations of the last millennium (v1.0), Geosci. Model Dev., 4, 33–45, https://doi.org/10.5194/gmd-4-33-2011, 2011.

Schröter, D., Cramer, W., Leemans, R., Prentice, I. C., Araújo, M. B., Arnell, N. W., Bondeau, A., Bugmann, H., Carter, T. R., Gracia, C. A., de la Vega-Leinert, A. C., Erhard, M., Ewert, F., Glendining, M., House, J. I., Kankaanpää, S., Klein, R. J. T., Lavorel, S., Lindner, M., Metzger, M. J., Meyer, J., Mitchell, T. D., Reginster, I., Rounsevell, M., Sabaté, S., Sitch, S., Smith, B., Smith, J., Smith, P., Sykes, M. T., Thonicke, K., Thuiller, W., Tuck, G., Zaehle, S., and Zierl, B.: Ecosystem Service Supply and Vulnerability to Global Change in Europe, Science, 310, 1333–1337, 2005.

Shimokawara, M., Nishimura, M., Matsuda, T., Akiyama, N., and Kawai, T.: Bound forms, compositional features, major sources and diagenesis of long chain, alkyl mid-chain diols in Lake Baikal sediments over the past 28,000 years, Org. Geochem., 41, 753–766, 2010.

Sicre, M.-A., Jalali, B., Martrat, B., Schmidt, S., Bassetti, M.-A., and Kallel, N.: Sea surface temperature variability in the North Western Mediterranean Sea (Gulf of Lion) during the Common Era, Earth Planet. Sc. Lett., 456, 124–133, 2016.

Sigl, M., Winstrup, M., McConnell, J. R., Welten, K. C., Plunkett, G., Ludlow, F., Buntgen, U., Caffee, M., Chellman, N., Dahl-Jensen, D., Fischer, H., Kipfstuhl, S., Kostick, C., Maselli, O. J., Mekhaldi, F., Mulvaney, R., Muscheler, R., Pasteris, D. R., Pilcher, J. R., Salzer, M., Schupbach, S., Steffensen, J. P., Vinther, B. M., and Woodruff, T. E.: Timing and climate forcing of volcanic eruptions for the past 2,500 years, Nature, 523, 543–549, 2015.

Sinninghe Damsté, J. S., Rampen, S., Irene, W., Rijpstra, C., Abbas, B., Muyzer, G., and Schouten, S.: A diatomaceous origin for long-chain diols and mid-chain hydroxy methyl alkanoates widely occurring in quaternary marine sediments: indicators for high-nutrient conditions, Geochim. Cosmochim. Ac., 67, 1339–1348, 2003.

Smith, M., De Deckker, P., Rogers, J., Brocks, J., Hope, J., Schmidt, S., Lopes dos Santos, R., and Schouten, S.: Comparison of U37K', TEX86H and LDI temperature proxies for reconstruction of south-east Australian ocean temperatures, Org. Geochem., 64, 94–104, 2013.

Spanish National Weather Agency – AEMet Open Data: AEMet Open Data, available at: http://www.aemet.es/es/datos_abiertos/AEMET_OpenData (last access: 19 December 2019), 2019.

Steinhilber, F., Beer, J., and Fröhlich, C.: Total solar irradiance during the Holocene, Geophys. Res. Lett., 36, L19704, https://doi.org/10.1029/2009GL040142, 2009.

Stuiver, M. and Quay, P. D.: Changes in Atmospheric Carbon-14 Attributed to a Variable Sun, Science, 207, 11–19, 1980.

Tejedor, E., Saz, M. Á., Cuadrat, J. M., Esper, J., and de Luis, M.: Temperature variability in the Iberian Range since 1602 inferred from tree-ring records, Clim. Past, 13, 93–105, https://doi.org/10.5194/cp-13-93-2017, 2017.

Theroux, S., D'Andrea, W. J., Toney, J., Amaral-Zettler, L., and Huang, Y.: Phylogenetic diversity and evolutionary relatedness of alkenone-producing haptophyte algae in lakes: Implications for continental paleotemperature reconstructions, Earth Planet. Sc. Lett., 300, 311–320, 2010.

Titos Martínez, M.: Los trabajos de desagüe de las lagunas de Sierra Nevada: un largo despropósito medioambiental, Revista del Centro de Estudios Históricos de Granada y su Reino, 223–243, 2019.

Titos Martínez, M. and Ramos Lafuente, A. J.: El refugio más antiguo de Sierra Nevada: Construido en 1891, aún se mantiene en pie, Andalucía en la historia, 48–53, 2016.

Trouet, V., Esper, J., Graham, N. E., Baker, A., Scourse, J. D., and Frank, D. C.: Persistent Positive North Atlantic Oscillation Mode Dominated the Medieval Climate Anomaly, Science, 324, 78–80, 2009.

Versteegh, G. J. M., Bosch, H. J., and De Leeuw, J. W.: Potential palaeoenvironmental information of C24 to C36 mid-chain diols, keto-ols and mid-chain hydroxy fatty acids; a critical review, Org. Geochem., 27, 1–13, 1997.

Villanueva, L., Besseling, M., Rodrigo-Gámiz, M., Rampen, S. W., Verschuren, D., and Sinninghe Damsté, J. S.: Potential biological sources of long chain alkyl diols in a lacustrine system, Org. Geochem., 68, 27–30, 2014.

Volkman, J. K., Barrett, S. M., and Blackburn, S. I.: Eustigmatophyte microalgae are potential sources of C29 sterols, C22–C28 n-alcohols and C28–C32 n-alkyl diols in freshwater environments, Org. Geochem., 30, 307–318, 1999.

Waters, C. N., Zalasiewicz, J., Summerhayes, C., Barnosky, A. D., Poirier, C., Gałuszka, A., Cearreta, A., Edgeworth, M., Ellis, E. C., Ellis, M., Jeandel, C., Leinfelder, R., McNeill, J. R., Richter, D. d., Steffen, W., Syvitski, J., Vidas, D., Wagreich, M., Williams, M., Zhisheng, A., Grinevald, J., Odada, E., Oreskes, N., and Wolfe, A. P.: The Anthropocene is functionally and stratigraphically distinct from the Holocene, Science, 351, aad2622, https://doi.org/10.1126/science.aad2622, 2016.

Willmott, V., Rampen, S. W., Domack, E., Canals, M., Sinninghe Damsté, J. S., and Schouten, S.: Holocene changes in Proboscia diatom productivity in shelf waters of the north-western Antarctic Peninsula, Antarct. Sci., 22, 3–10, 2010.

Yu, M., Zhang, H., Li, L., and Zhao, M.: Spatial Distributions and Potential Sources of Long Chain (C30, C32 1,15-) Alkyl Diols in Surface Sediments from Eastern China Marginal Seas, J. Ocean U. China, 17, 1114–1122, 2018.